HHS Public Access

Author manuscript

Biochem J. Author manuscript; available in PMC 2019 October 15.

Published in final edited form as:

Biochem J. ; 476(8): 1247–1266. doi:10.1042/BCJ20180394.

Regulation of differential proton-coupled folate transporter gene expression in human tumors: transactivation by KLF15 with NRF-1 and the role of Sp1

Zhanjun Hou[1,2], **Carrie O'Connor**[2], **Josephine Frühauf**[2], **Steve Orr**[2], **Seongho Kim**[1,2], **Aleem Gangjee**[3], **Larry H. Matherly**[1,2,4]

[1]Molecular Therapeutics Program, Barbara Ann Karmanos Cancer Institute, Wayne State University School of Medicine, Detroit, MI, U.S.A.;

[2]Department of Oncology, Wayne State University School of Medicine, Detroit, MI, U.S.A.;

[3]Division of Medicinal Chemistry, Duquesne University, Pittsburgh, PA, U.S.A.;

[4]Department of Pharmacology, Wayne State University School of Medicine, Detroit, MI, U.S.A.

Abstract

Tumors can be therapeutically targeted with novel antifolates (e.g. AGF94) that are selectively transported by the human proton-coupled folate transporter (hPCFT). Studies were performed to determine the transcription regulation of hPCFT in tumors and identify possible mechanisms that contribute to the highly disparate levels of hPCFT in HepG2 versus HT1080 tumor cells. Transfection of hPCFT-null HT1080 cells with hPCFT restored transport and sensitivity to AGF94. Progressive deletions of the hPCFT promoter construct (−2005 to +96) and reporter gene assays in HepG2 and HT1080 cells confirmed differences in hPCFT transactivation and localized a minimal promoter to between positions −50 and +96. The minimal promoter included KLF15, GC-Box and NRF-1 *cis*-binding elements whose functional importance was confirmed by promoter deletions and mutations of core consensus sequences and reporter gene assays. In HepG2 cells, NRF-1, KLF15 and Sp1 transcripts were increased over HT1080 cells by ~5.1-, ~44-, and ~2.4-fold, respectively. In *Drosophila* SL2 cells, transfection with KLF15 and NRF-1 synergistically activated the hPCFT promoter; Sp1 was modestly activating or inhibitory. Chromatin immunoprecipitation and electrophoretic mobility shift assay (EMSA) and supershifts confirmed differential binding of KLF15, Sp1, and NRF-1 to the hPCFT promoter in HepG2 and HT1080 cells that paralleled hPCFT levels. Treatment of HT1080 nuclear extracts (NE) with protein kinase A increased Sp1 binding to its consensus sequence by EMSA, suggesting a role for Sp1 phosphorylation in regulating hPCFT transcription. A better understanding of determinants of hPCFT transcriptional control may identify new therapeutic strategies for cancer by modulating hPCFT levels in combination with hPCFT-targeted antifolates.

Correspondence: Zhanjun Hou (houz@karmanos.org) or Larry H. Matherly (matherly@karmanos.org).

Author Contribution

Z.H. and L.H.M. designed the study and wrote the paper. Z.H., C.O., J.F., and S.O. performed experiments and analyzed the data. S.K. performed part of the statistical analysis. A.G. provided the hPCFT-targeted compound AGF94.

Competing Interests

The Authors declare that there are no competing interests associated with the manuscript.

Introduction

The human proton-coupled folate transporter (hPCFT) was discovered in 2006 and was identified as the principal folate transporter involved in the intestinal absorption of dietary folates [1]. Loss-of-function mutations in hPCFT resulting in mutant or absent protein account for the rare auto-somal inherited disorder, hereditary folate malabsorption [2].

While hPCFT is broadly expressed in human tumor cells [3] including primary specimens [4–6], it is undetectable in most leukemias [3,7] and even for tumor types typically associated with high levels of hPCFT, specimens were detected with low levels of expression [3–6]. Particular interest has focused on hPCFT transport of pemetrexed (PMX; Alimta), given its excellent substrate activity for hPCFT [8,9] and its role in treating malignancies, including malignant pleural mesothelioma [10] and non-small cell lung cancer (NSCLC) [11]. In malignant pleural mesothelioma treated with PMX, patients with low levels of hPCFT had lower rates of disease control and shorter overall survival [4], suggesting that hPCFT is an important determinant of clinical efficacy of PMX in this disease.

Studies have begun to examine the transcriptional regulation of hPCFT in order to better understand the basis for variations in hPCFT levels between tissues including malignant cells. The hPCFT promoter is GC rich and includes a large (1085 bp) CpG island which spans the transcriptional start site and can be hypermethylated, resulting in low levels of hPCFT expression. Treatment of human leukemia (i.e. CCRF-CEM, Jurkat) [7], methotrexate (MTX)-resistant HeLa [12], and malignant mesothelioma [4] cells with the DNA methyltransferase inhibitor 5-aza-2′-deoxycytidine (5-Aza) resulted in the substantial restoration of hPCFT mRNA expression. For malignant mesothelioma, this was accompanied by increased sensitivity to PMX [4]. Other studies have begun to explore roles for specific transcription factors and *cis*-elements in regulating hPCFT, including Sp1, AP2, NRF-1, KLF4, HNF4α and vitamin D [13–16]. The hPCFT minimal promoter was localized to between positions −42 and +96 (relative to the transcriptional start site at position +1) [12], including certain of these elements. Although modest transactivation of hPCFT by NRF-1 was suggested [13], mechanisms that contribute to differences in hPCFT between tumor cells are unclear.

In recent years, the notion of hPCFT drug targeting has been extended to a new generation of tumor-targeted 6-substituted pyrrolo[2,3-*d*]pyrimidine compounds that are structurally and functionally distinct from PMX, and that exhibit near exclusive transport by hPCFT under acidic pH conditions characterizing many tumors [17]. For AGF94, the hPCFT-targeted prototype of this series [17,18], this manifests as high levels of selective drug uptake by tumors over normal tissues and potent inhibition of *de novo* purine nucleotide biosynthesis (at glycinamide ribonucleotide formyltransferase, the first folate-dependent step), resulting in *in vitro* and *in vivo* anti-tumor efficacy.

With the development of hPCFT-targeted therapies [17] for cancer, there is growing interest in critical determinants of transcriptional control for hPCFT. In this study, we explore the mechanistic bases for the transcription regulation of hPCFT in tumors. Our goal was to better understand the role of differences in hPCFT gene expression in determining

sensitivities of HepG2 and HT1080 human tumor cells to hPCFT-targeted antifolates. Insights into these regulatory processes may lead to entirely new strategies to enhance the therapeutic efficacies of novel hPCFT-targeted drugs.

Materials and methods

Chemicals and reagents

AGF94 [(S)-2-((5-[3-(2-amino-4-oxo-4,7-dihydro-3H-pyrrolo[2,3-*d*]pyrimidin-6-yl)-propyl]-thio-phene-2-car-bonyl)-amino)-pentanedioic acid] was synthesized, as previously described [18]. Leucovorin [(6R,S) 5-formyl tetrahydrofolate] was obtained from the Drug Development Branch, National Cancer Institute, Bethesda, MD. [3′,5′,7-^{3}H]MTX (20 Ci/mmol) was purchased from Moravek Biochemicals (Brea, CA). 5-Aza-2′-deoxycytidine (5-Aza) was purchased from Sigma–Aldrich (St. Louis, MO). Restriction and modifying enzymes were purchased from New England Biolabs (Ipswich, MA). The mammalian expression vector pcDNA3.1/myc-His(–)A was purchased from Invitrogen (Carlsbad, CA). Reporter gene vectors pGL3-Basic and pGL4.74[hRluc/TK] were purchased from Promega (Madison, WI). Other chemicals were obtained from commercial sources in the highest available purities.

Construction of expression constructs luciferase plasmids and site-directed mutagenesis

The NRF-1 cDNA was amplified from HeLa cells by RT-PCR, followed by digestion with XhoI and KpnI, and cloning into pcDNA3.1/myc-His(–)A (NRF-1$^{\text{Myc-His6}}$/pcDNA3.1). KLF15$^{\text{Myc-His6}}$/pcDNA3.1 was generated by digesting hKLF15/pcDNA3.1His+C (a gift from Dr. Otteson [19]) with BamHI and HindIII and subcloning into pcDNA3.1/myc-His(–)A. Sp1/pcDNA3.1 was generated by digesting the pPacSp1 plasmid construct [provided by Dr. Robert Tijan (University of California, Berkeley, CA)] with NheI and XhoI and subcloning into pcDNA3.1/myc-His(–)A. All site-directed mutagenesis used the QuickChange II Site-Directed Mutagenesis Kit (Agilent Technologies Inc., Santa Clara, CA). For *Drosophila* SL2 transfection experiments (below), BamHI and XhoI sites were introduced immediately 5′ and 3′ of the NRF-1 insert in the NRF-1/pcDNA3.1 construct by site-directed mutagenesis, followed by digestion and subcloning into the pPacO vector between the BamHI and XhoI sites (pPacNRF-1). Similarly, to prepare pPacKLF15, a XhoI site was introduced 3′ of the KLF15 insert in KLF15/pcDNA3.1, followed by digestion and subcloning.

A −2005/+96 hPCFT promoter fragment was amplified from HeLa genomic DNA and subcloned into pGL3-Basic vector between KpnI and XhoI (hPCFT−2005/+96/pGL3). Progressively deleted constructs (hPCFT −1613/+96/pGL3, hPCFT−1209/+96/pGL3, hPCFT−807/+96/pGL3, hPCFT−386/+96/pGL3, and hPCFT−82/+96/pGL3) were generated by introducing KpnI restriction sites at the desired locations in hPCFT−2005/+96/pGL3, followed by KpnI digestion and religation. Other progressively deleted hPCFT promoter constructs were prepared by direct deletions using QuickChange mutagenesis (i.e. hPCFT −40/+96/pGL3, hPCFT−20/+96/pGL3, and hPCFT−10/+96/pGL3 were generated from hPCFT−82/+96/pGL3; hPCFT−35/+96/pGL3 was generated from hPCFT−40/+96/pGL3; and hPCFT−15/+96/pGL3 was generated from hPCFT−20/+96/pGL3). hPCFT −50/+96/

pGL3 was prepared from hPCFT−40/+96/pGL3 by direct insertion of additional sequence by QuickChange mutagenesis. The hPCFT core promoter constructs −50/+96 was used as a template to mutate the consensus sequence of NRF-1, KLF15, and GC-Box, resulting in hPCFT−50/+96/NRF-1m, hPCFT−50/+96/KLF15m, and hPCFT−50/+96/GC-Boxm, respectively. The hPCFT−50/+96/NRF-1m construct was used to generate double mutations of the NRF-1 and KLF15 consensus sequences (hPCFT−50/+96/NRF-1m/KLF15m).

All constructs were confirmed by Sanger sequencing by Genewiz (South Plainfield, NJ). Primers used for the mutations, deletions or insertions were purchased from Invitrogen and are listed in Supplementary Table S2.

Cell culture

The human HT1080 fibrosarcoma and HepG2 hepatocellular carcinoma cell lines were obtained from American Type Culture Collection (Manassas, VA). Wild-type (WT) and hPCFT-null R1–11 HeLa cells were gifts of Dr. I. David Goldman (Albert Einstein College of Medicine, Bronx, NY) [9]. *Drosophila* SL2 cells were a gift of Dr. Bonnie Sloane (Wayne State University, Detroit, MI). The HT1080, HepG2, and hPCFT-null R1–11 HeLa cell lines were cultured in complete RPMI-1640 medium containing 10% fetal bovine serum (Sigma, St. Louis, MO), 2 mM L-glutamine, 100 units/ml penicillin, and 100 μg/ml streptomycin in a humidified atmosphere at 37°C in the presence of 5% CO_2 and 95% air. SL2 cells were maintained in Schneider's *Drosophila* Medium (Life Technologies Corporation, Carlsbad, CA), supplemented with 10% fetal bovine serum and 2 mM L-glutamine, 100 units/ml penicillin, and 100 μg/ml streptomycin at 25°C.

HepG2 and HT1080 cells were transfected with expression constructs [hPCFT$^{Myc\text{-}His6}$/pcDNA3.1 [20], NRF-1$^{Myc\text{-}His6}$/pcDNA3.1, KLF15$^{Myc\text{-}His6}$/pcDNA3.1, Sp1/pcDNA3.1] using Lipofectamine 2000 reagent (Invitrogen, Carlsbad, CA) as described [21]. For stable transfections, cultures were treated with G418 (1000 μg/ml for HT1080; 2000 μg/ml for HepG2) beginning 48 h post-transfection.

HepG2 cells were also transfected with siRNA for NRF-1 [ON-TARGETplus Human NRF-1 (4899) siRNA #2], KLF15 [ON-TARGETplus Human KLF15 (28999) siRNA – SMARTpool], and Sp1 [ON-TARGETplus Human Sp1 (28999) siRNA – SMARTpool] using DharmaFECT4 Transfection Reagent. siRNAs and transfection reagent were purchased from Dharmacon (Lafayette, CO). The transfections were performed according to our optimized protocol based on the manufacturer's instructions, with siRNA at a final concentration of 50 nM and 7.5 μl DharmaFECT4 per transfection (total 400 μl). The samples were assayed 24 h post-transfection.

For cell proliferation assays, HepG2, HT1080, and stable hPCFT-transfected HT1080/hPCFT cells were plated in 96-well culture plates (4000 cells/well; 200 ml/well) with folate-free RPMI-1640 and dialyzed fetal bovine serum (Sigma), L-glutamine, and antibiotics, supplemented with 2 nM leucovorin. AGF94 was added at a final concentration from 1 to 1000 nM. Cells were incubated from 96 to 120 h (depends on the cell line) at 37°C in a CO_2 incubator. Cell viabilities were measured with a fluorescence-based viability assay (CellTiter-Blue, Promega) and a fluorescence plate reader (emission at 590 nm, excitation at

560 nm) for calculating the drug concentrations that inhibit growth by 50% (IC_{50}). Prior to experiments, all cell lines were grown in folate-free RPMI-1640 (Life Technologies), supplemented with 10% fetal bovine serum, 100 units/ml penicillin, and 100 μg/ml streptomycin, and 2 mM L-glutamine for at least 2 weeks.

Real-time RT-PCR analysis

RNAs were isolated from the cell cultures using TRIzol reagent (Life Technologies, Carlsbad, CA). cDNAs were synthesized with random hexamers and MuLV reverse transcriptase (including RNase inhibitor) (Applied Biosystems, Waltham, MA) and purified using a QIAquick PCR Purification Kit (Qiagen, Valencia, CA). Quantitative real-time RT-PCR was performed using a Roche LightCycler 480 (Roche Diagnostics, Indianapolis, IN) with gene-specific primers for hPCFT, KLF15, NRF-1, and Sp1 and appropriate probes (Roche Diagnostics), and a LightCycler 480 Probes Master kit (Roche Diagnostics, Indianapolis, IN), or with gene-specific primers and a LightCycler 480 SYBR Green I Master kit (Roche Diagnostics, Indianapolis, IN). Transcript levels were normalized to those for glyceraldehyde-3-phosphate dehydrogenase (GAPDH) and/or β-actin. For relative hPCFT gene copy quantitation, genomic DNAs were isolated using TRIzol (Invitrogen) and analyzed by RT-PCR with RNase P as an endogenous reference gene. Primer sequences are summarized in Supplementary Table S1.

Western blot analysis

R1–11, HepG2, HT1080, and HT1080/hPCFT cell lines were cultured, as described above. Cells (~2×10^7) were disrupted by sonication and cell debris was removed by centrifugation (1,800 rpm, 5 min). A particulate membrane fraction was prepared by centrifugation (37,000×*g*, 30 min). The membrane pellet was solubilized with 1% SDS in 10 mM Tris–HCl [pH 7, containing protease inhibitors (Roche Diagnostics)]. Membrane proteins (120 μg) were electrophoresed on 7.5% Tris/glycine gels with SDS [22] and transferred to polyvinylidene difluoride membranes (Thermo Scientific, Rockford, IL) [23]. To detect hPCFT, the hPCFT-specific polyclonal antibody raised in rabbits to a carboxyl termini peptide [24] was used at a titer of 1 : 2,000. Protein loading was normalized to levels of β-actin using anti-β-actin mouse antibody (Sigma–Aldrich). IRDye800CW-conjugated goat anti-rabbit IgG or IRDye800CW-conjugated goat anti-mouse IgG (LI-COR Biosciences, Lincoln, NE) was used as the secondary antibody. Membranes were scanned with an Odyssey infrared imaging system (LI-COR Biosciences, Omaha, NE).

hPCFT transport assay

hPCFT transport assays in monolayer cultures were performed as described [20,24]. R1–11, HepG2, HT1080, and HT1080/hPCFT stable transfectant cells were plated at 30–40% confluence into 60-mm dishes in complete RPMI-1640 (above). After 48 h, cellular uptakes of [^{3}H]MTX (at 0.5 mmol/L) were measured over 5 min at 37°C in MES-buffered saline (20 mmol/L MES, 140 mmol/L NaCl, 5 mmol/L KCl, 2 mmol/L $MgCl_2$, and 5 mmol/L glucose, pH 5.5). The dishes were washed 3× with ice-cold phosphate-buffered saline. The cells were solubilized in 0.5 N NaOH and radioactive contents and protein concentrations [25] of the alkaline cell homogenates were determined. Intracellular radioactivity was calculated in units of pmol [^{3}H]MTX per mg of cell protein.

Transient transfections and luciferase assays

For transient transfections of HepG2 and HT1080 cells, 1 μg of hPCFT-luciferase reporter gene in pGL3 vector or 'promoter-less' pGL3-Basic plasmid was co-transfected with 200 ng of pGL4.74[hRluc/TK] vector using Lipofectamine 2000 reagent (Invitrogen) as described [21]. Forty-eight hours post-transfection, cells were harvested, and lysates were prepared according to the manufacturer's instructions (Dual-Luciferase Reporter Assay System, Promega). Firefly luciferase activities were assayed with the Dual-Luciferase Reporter Assay System and a Synergy 2 Microplate Reader (BioTek), with results normalized to *Renilla* luciferase activity.

Drosophila SL2 cells were co-transfected with 2 μg of the hPCFT-luciferase reporter gene constructs and 200 ng of the pPacO (empty vector), Sp1 (pPacSp1), Sp3 [pPacUSp3 (Sp3 longer form), pPacSp3 (Sp3 shorter form) [26,27]], NRF-1 (pPacNRF-1), or KLF15 (pPacKLF15) cDNA constructs, using FuGENE 6 transfection reagent (Promega, Madison, WI), according to the manufacturer's recommendations. The pPacSp1 and pPacO plasmid constructs were provided by Dr. Robert Tijan (University of California, Berkeley, CA), and the pPacSp3 and pPacUSp3 constructs were provided by Dr. Guntram Suske (Philipps-University, Marburg, Germany). For experiments in which results for transfections with two transcription factor constructs were directly compared with results for cells transfected with a single transcription factor construct, total DNA amounts were maintained constant by adding empty pPacO to the single transfections. Cells were harvested after 48 h for luciferase assays using a single-luciferase assay system (Promega) with a microplate reader (BioTek). Luciferase activities were normalized to cellular proteins and measured by the Bio-Rad protein assay system.

CpG methylation analysis by bisulfite sequencing

R1–11 HeLa, HT1080 and HepG2 cells were plated in 60-mm dishes (0.5×10^6 cells/dish) in complete RPMI-1640 medium (above), two dishes for each cell line. Each cell line was treated with 2 μM 5-Aza or DMSO for 72 h; the 5-Aza was replaced with fresh drug every 24 h. After 5-Aza treatments, the cells were passed into 100-mm dishes and after 48 h, cells were harvested for isolation of genomic DNAs (below), and for RNA extraction and gene expression analysis by real-time RT-PCR.

Genomic DNAs were isolated using TRIzol (Invitrogen). The EpiTect Bisulfite Kit (Qiagen) was used for bisulfite conversion and cleanup of DNAs for methylation analysis. Amplification of CpG sequence (−74 to +229) used primer 1 (5′-GAGAGTTYGGTGGTTTTAGGTTATAGG-3′; Y = A/T) and primer 2 (5′-TAATAAA CRAACCCTACAAAACCAAAACAAAATTAAC-3′; R = G/C), as described [7,12]. PCR conditions were 94°C for 5 min, 35 cycles of 94°C for 30 sec, 58°C for 30 sec, and 72°C for 1 min, followed by 1 cycle of 72°C for 10 min. TaKaRa EpiTaq™ HS (Takara Bio Inc.) was used to amplify bisulfite converted DNA. The 302 bp amplicons were resolved on a 1% agarose gel, gel purified (QIAEX II Gel Extraction Kit, Qiagen), and cloned into pCRII-TOPO vector (Invitrogen). Plasmid DNAs from 10–16 bacterial clones were prepared for Sanger DNA sequencing by Genewiz. Sequencing results were compared with hPCFT genomic sequence with the QUantification tool for Methylation Analysis or QUMA (http://

quma.cdb.riken.jp/) for calculation of the extent of CpG methylation for the −74/+229 hPCFT promoter region.

Chromatin immunoprecipitation (ChIP) assays

ChIP assays were carried out with the ChIP-IT High Sensitivity kit in combination with the ChIP-IT qPCR Analysis kit, both obtained from Active Motif (Carlsbad, CA). ChIP assays were performed in HepG2 and HT1080 cells, according to the manufacturer's instructions, with antibodies to NRF-1 (Abcam, Cat# ab34682), KLF15 (Sigma–Aldrich, Cat# SAB5300174), and Sp1 (Active Motif, Cat# 39058). The Mouse IgG2a [MOPC-3] Isotype (Abcam, Cat# ab18413) was used as a negative control in the pull-down steps. Briefly, HepG2 and HT1080 cells (~1.5×10^7) were fixed with a specially formulated formaldehyde buffer at room temperature for 15 min. Fixed cells were collected and homogenized. DNA was sheared into small fragments by sonication, then incubated with anti-NRF-1, KLF15 or Sp1 antibody. The antibody-bound protein/DNA complexes were immunoprecipitated with Protein G agarose beads and washed via gravity filtration. Following immunoprecipitation, DNA cross-links were reversed, proteins were removed by Proteinase K digestion, and the DNA was recovered and purified. The ChIP DNA and input DNA obtained were then used for qPCR analyses with the 'DNA Standards, design and analysis template' provided by ChIP-IT qPCR Analysis kit. The qPCRs were performed using a Roche LightCycler 480 and LightCycler 480 SYBR Green I Master Kit Mix (Roche Diagnostics), with primers located in the hPCFT core promoter region that includes putative binding sites for NRF-1, KLF15 or Sp1. Primer sequences are summarized in Supplementary Table S2.

Electrophoretic mobility shift assay (EMSA)

Nuclear extracts (NE) from HT1080 and HepG2 cells were prepared with a Nuclear Extraction Kit from Active Motif, according to the manufacturer's instructions. Final NE protein concentrations were determined by the Bio-Rad protein assay. NE proteins (5 μg) from HT1080 and HepG2 cells were used for each reaction. Complementary single-stranded oligonucleotides were purchased from Invitrogen, and were annealed by heating the mixed oligonucleotides in Duplex Buffer (100 mM potassium acetate; 30 mM HEPES, pH 7.5) to 94°C for 5 min, followed by gradual cooling. IRDye700-labeled double-stranded oligonucleotides were purchased from Integrated DNA Technologies, Inc. (Coralville, IA). Oligonucleotide sequences are provided in Supplementary Table S3. The Odyssey Infrared EMSA Kit was purchased from LI-COR (Lincoln, NE). For detection of the DNA-Sp1 and -KLF15 protein complexes, NE proteins were pre-incubated at room temperature in a reaction solution containing 10 mM Tris–HCl (pH 7.5), 50 mM KCl, 3.5 mM DTT, 5 mM $MgCl_2$, 0.25% Tween, and 1 μg of poly(dI-dC). To study the binding of NRF-1 to the hPCFT core promoter element, the same binding buffer components (above) were used, but with 1 μg of poly(dA-dT) (InvivoGen) rather than poly(dI-dC). Competitor oligonucleotides (50~500 nM) were added, as appropriate. After incubating for 10 min at room temperature, the IRDye700-labeled duplex oligonucleotide was added, and the reaction was incubated for another 30 min at room temperature. For supershift experiments, 1~2 μg of antibody to NRF-1 (Abcam, Cat# ab34682), KLF15 (Sigma–Aldrich, Cat# SAB5300174) or Sp1 (Active Motif, Cat# 39058) was added to the reaction mixtures and incubated for 20 min at 4°C (for NRF-1 and KLF15) or 40 min at 25°C (for Sp1). DNA–protein complexes were

supplemented with Orange Loading Dye (LI-COR) and separated on 5% TGE native acrylamide gel (containing 50 mM Tris, pH 7.5; 0.38 M glycine; and 2 mM EDTA) in 0.5× TGE buffer at 4°C and 80 V. The complexes were visualized by an Odyssey infrared imaging system (LI-COR Biosciences).

For some experiments, HT1080 NE proteins (70 μg) were incubated with or without 28 units of protein kinase A catalytic subunit (Sigma) in 50 mM Tris (pH 7.5), 10 mM $MgCl_2$, and 10 μM ATP at 30°C for 1 h in a total volume of 70 μl. Five micrograms of the treated NE proteins were used for EMSA, as described above.

Statistical analysis

Statistical analyses were performed using GraphPad Prism version 6.07 for Windows (GraphPad Software, La Jolla, CA, U.S.A.). Differences between two groups were statistically assessed using the Mann–Whitney *U* test. Univariate associations of NRF-1, KLF15, and Sp1 with hPCFT were examined using log-transformed transcript levels by Pearson's correlation and plotted with linear regression by Prism. Since univariate association analyses do not distinguish between direct and indirect associations, multivariate regulatory association analyses were further performed between hPCFT and three transcription factor genes using the maximum relevance minimum redundancy backward (MRNETB) method with Pearson's correlations [28,29]. MRNETB is a regulatory network inference approach based on the mutual information matrix with a backward elimination and a sequential replacement. As a reference, univariate and multivariate associations were further assessed using Spearman's correlations and the results were consistent with those of Pearson's correlations. The R/Bioconductor packages *minet* and *igraph* were used to generate the inferred regulatory network [28,29].

Results

hPCFT gene expression in HT1080 is significantly down-regulated compared with HepG2 cells and is independent of hPCFT gene copy or promoter sequence alterations

Although hPCFT is broadly expressed among many solid tumor cell lines of different lineages, there were significant variations in hPCFT levels [3]. We selected HepG2 (high hPCFT) and HT1080 (negligible hPCFT) [3] as cell line prototypes to begin to explore the possible molecular determinants of disparate hPCFT gene expression among solid tumors. The nearly complete loss of hPCFT transcripts in HT1080 cells (comparable to hPCFT levels in hPCFT-null R1–11 HeLa cells [9]) (Figure 1A) was accompanied by a lack of detectable hPCFT protein on Western blots (Figure 1B) and very low levels of uptake of [^{3}H]MTX (a surrogate transport substrate for hPCFT) at pH 5.5 (the hPCFT optimum [8]) (Figure 1C). No differences in hPCFT gene copy were detected between HepG2 and HT1080 cells by quantitative PCR (Supplementary Figure S1). Furthermore, no sequence differences in ~ 2000 bp upstream of the hPCFT transcriptional start site were identified between HepG2 and HT1080 cells (data not shown).

As expected, HT1080 cells were less sensitive to the anti-proliferative effects of the hPCFT-targeted antifolate inhibitor AGF94 [18] than were HepG2 cells (Figure 1D). Stable

transfection of HT1080 cells with hPCFT cDNA restored substantial expression of the hPCFT protein (Figure 1B) and hPCFT transport activity (Figure 1C), resulting in increased AGF94 sensitivity (Figure 1D).

Role of CpG methylation in the loss of hPCFT gene expression in HT1080 cells

Based on reports that losses of hPCFT in malignant cells are frequently associated with hypermethylation of the hPCFT promoter [4,7,12], we initially tested whether the very low level of hPCFT gene expression in HT1080 cells could also be attributed to promoter hypermethylation. For these experiments, we treated H1080 cells, along with R1–11 HeLa and HepG2 cells, with the CpG demethylating agent 5-Aza.

To confirm hPCFT promoter methylation status (including any changes in promoter methylation with 5-Aza treatment), genomic DNAs were isolated and converted by bisulfite treatment and purified. Bisulfite-treated genomic DNAs were PCR-amplified with degenerate primers flanking positions −74 and +229 spanning the transcriptional start site (position +1), a region previously reported to be heavily methylated accompanying loss of hPCFT expression [4,7,12]. The amplicons (302 bp) were gel-purified, subcloned (PCRII-TOPO) and the plasmids were isolated from 10–16 bacterial clones for Sanger sequencing to calculate the percentage of methylated CpGs between positions −74 and +229 (Figure 1E).

For untreated cells, the 37 CpGs in the −74 to +229 segment were heavily methylated in R1–11 cells (69.2%), less so in HT1080 cells (49.1%), and minimally methylated in HepG2 cells (1.62%). 5-Aza treatment decreased methylation from 69.2% to 29.0% for R1–11 cells, accompanying 8.4-fold increased levels of hPCFT transcripts (Figure 1A), as previously reported [12]. Changes in CpG methylation with 5-Aza treatment were from 49.1% to 31.3% for HT1080 cells, and from 1.62% to 0.74% for HepG2 cells. These were not accompanied by statistically significant changes in hPCFT transcript levels (Figure 1A).

Thus, while our results do suggest that there are substantial differences in CpG methylation between HepG2 and HT1080 cells, these are incompletely reversed by 5-Aza and the losses in CpG methylation in HT1080 cells were not accompanied by increased hPCFT. The very low level of hPCFT gene expression in HT1080 cells appears to be only modestly attributed to CpG hypermethylation. Involvement of histone deacetylation in hPCFT gene expression in HT1080 cells was also ruled out as causal since treatment with valproic acid (VPA; 1 mM for 72 h; with our without 5-Aza) did not alter the hPCFT transcript levels in HT1080 cells (data not shown).

Mapping of hPCFT core promoter region and identification of critical transcription *cis*-elements

A 2.1 kb hPCFT (−2005/+96) promoter reporter construct (positions −2005 to +96; transcription starts at +1) was PCR-amplified from HeLa cells and subcloned in pGL3-Basic plasmid. A series of progressive deletions was introduced in the −2005/+96 construct (−1613/+96, −1209/+96, −807/+96, −386/+96, −82/+96, −50/+96, −35/+96, −20/+96, −15/+96, and −10/+96) (Figure 2A). The full-length and promoter deletion constructs were transiently transfected into HepG2 and HT1080 cells for luciferase reporter assays. Firefly luciferase activities were normalized to those for *Renilla* luciferase.

The −2005/+96 pGL3 promoter construct showed a high level of activity in HepG2 cells that was relatively constant upon deleting >1900 bp of upstream sequence to position −50 (−50/+96 construct) (Figure 2A). Additional deletion from position −35 (−35/+96) to −15 (−15/+96) decreased activity by ~58%, whereas activity further decreased (~86%) with deletion to position −10 (−10/+96). This implies that the −50/+96 promoter construct approximates a minimal core promoter, in agreement with published findings of Goldman and colleagues who localized a minimal hPCFT promoter sequence to between positions −42 and +96 [12].

hPCFT promoter activity measured in HT1080 cells paralleled the low levels of hPCFT transcripts in these cells and was ~25–50% of that measured for HepG2 cells for the −2005/+96 to −50/+96 constructs but fell to ~15% of HepG2 activity levels for −35/+96 construct. These results strongly suggest that losses of hPCFT transcripts and protein in HT1080 cells were primarily due to a transcriptional defect.

The profound losses of hPCFT promoter activity in both HepG2 and HT1080 cells upon deletions from positions −50 (−50/+96) to −35 (−35/+96) and from positions −15 (−15/+96) to −10 (−10/+96) (Figure 2A) likely reflect the presence of essential cis-elements in these regions. Bioinformatics analysis (MatInspector [30]) at high stringency revealed three putative transcription factor binding sites from positions −50 to +1 within the hPCFT core promoter (−50/+96) region, including KLF15 (−48 to −29), GC-Box (−30 to −14), and NRF-1 (−15 to +1) elements (Figure 2B). From the patterns of luciferase activity recorded, the dramatic losses of promoter activity upon deletion from positions −50 to −35, and from positions −15 to −10, may reflect the removal of KLF15 and NRF-1-binding sites, respectively. Although a putative GC-Box was also identified, as noted above, deletion across this region had a minimal deleterious effect on luciferase activity. Of these three elements, only the NRF-1 site was previously reported [13].

To further explore the potential importance of the KLF15, GC-Box, and NRF-1-binding sites on hPCFT promoter activity, we mutated these elements within the hPCFT core promoter (−50/+96) construct (Figure 2B). Mutant reporter constructs were transiently transfected into HepG2 and HT1080 cells, followed by luciferase reporter assays, with results compared with the WT promoter. Interestingly, mutations caused somewhat different impacts between the cell lines such that mutation of the KLF15-binding site resulted in 42% (in HT1080) and 80% (in HepG2) losses of luciferase activity, whereas the NRF-1 mutation caused 68% (in HT1080) and 89% (in HepG2) decreases in luciferase activity (Figure 2A). When both KLF15 and NRF-1 *cis*-elements were mutated, losses of luciferase activity were augmented, decreasing to ~10% and ~5% of WT promoter levels in HT1080 and HepG2 cells, respectively. For the GC-Box, mutation of the core binding sequence resulted in a modest activation (~26%) of promoter activity in HepG2 cells but not in HT1080 cells (see below). All mutations affected the loss of transcription factor binding to their binding sites, as reflected in results of EMSA (Figure 5B).

Levels of endogenous KLF15, NRF-1, and Sp1 expression in HepG2 and HT1080 cells and the impact of NRF-1, KLF15, and Sp1 overexpression and knock-down on hPCFT gene expression

The aforementioned results (Figure 2A) suggested potentially important regulatory roles for KLF15 and NRF-1, and possibly Sp1, in regulating hPCFT gene transcription. Although a regulatory role for NRF-1 in hPCFT transcription was previously suggested for HeLa cells [13], regulation of hPCFT by KLF15 has not been previously described.

When NRF-1, KLF15 and Sp1 transcript levels were measured in HepG2 and HT1080 cells, striking differences were detected (~5.1-, ~44- and ~2.4-fold, respectively; HepG2>>HT1080) (Figure 3A). Combined with the results of the reporter gene assays in Figure 2A, these findings imply that NRF-1 and KLF15 play critical roles in regulating hPCFT gene expression from the minimal promoter. The substantial differences in levels of these transcription factors likely contribute to the disparate hPCFT amounts in HepG2 versus HT1080 cells, although any role of Sp1 appears to be more subtle.

To further study the roles of NRF-1, KLF15 and Sp1 on hPCFT promoter activity, we stably overexpressed NRF-1, KLF15 or Sp1 (in pcDNA3.1 vector; with Myc-His6 tag for KLF15 and NRF-1) in both HepG2 and HT1080 cells. Transfection was monitored by real-time RT-PCR and was reflected in increased NRF-1, KLF15, and Sp1 transcript levels over background levels. Increased levels of KLF15 (~5-fold) and NRF-1 (~1.5-fold) transcripts were accompanied by statistically significant increases in hPCFT transcript levels (~40–50%) in HepG2 cells; however, increased levels of Sp1 (~1.4-fold) resulted in decreased hPCFT transcript levels (~40%) (Figure 3B). This is consistent with the observations of increased luciferase activity in HepG2 cells transfected with the mutant −50/+96/GC-Boxm construct (Figure 2A). However, for HT1080 cells there was no impact on hPCFT gene expression, although increased levels of KLF15 (~14-fold), NRF-1 (~3.5-fold) and Sp1 (~1.5-fold) were measured (Figure 3C). We also knocked-down expression of NRF-1, KLF15, and Sp1 in HepG2 cells to study the impact on hPCFT gene expression with siRNAs. We knocked-down gene expression of NRF-1, KLF15 and Sp1 in HepG2 by ~50%, ~80%, and ~65%, respectively, with siRNA. Only for NRF-1, was the knock-down associated with decreased (~25%) hPCFT transcript levels (Supplementary Figure S2).

To test if there was coordinate multi-factorial regulation of hPCFT gene expression by these transcription factors in HT1080 cells, we transiently transfected NRF-1, KLF15 or Sp1 singly or in combination (i.e. NRF-1 + KLF15, NRF-1 + Sp1, KLF15 + Sp1, and NRF-1 + KLF15 + Sp1). As shown in Figure 3D, no significant impact on hPCFT gene expression was measured in HT1080 cells with overexpression of NRF-1, KLF15, or Sp1 singly or in combination.

Collectively, these results strongly suggest a multi-factorial regulation of hPCFT gene expression including NRF-1, KLF15, and Sp1, along the potential effects of other factors not considered in this report. Another critical determinant could involve potential posttranslational modifications of critical factors (see below).

Functional analysis of hPCFT core promoter elements and transcription factors in *Drosophila* SL2 cells

The hPCFT minimal promoter includes a GC-Box (positions −30 to −14; Figure 2B) that resides between the KLF15 (−48 to −29) and NRF-1 (−15 to +1) binding sites implicated as functionally important in regulating hPCFT promoter activity (Figure 2B). Whereas deletion of the GC-Box (−20/+96 and −15/+96; Figure 2A) does not impact promoter activity in HepG2 cells, its mutation resulted in an activation (26%) of promoter activity (Figure 2A). KLF15 and Sp1 are reported to synergistically activate gene expression of the LRP5 and AceCS2 genes [31,32] and for AceCS2, synergistic transactivation correlates with an ability of KLF15 to stably interact with Sp1 [32]. Furthermore, NRF-1 binding to the common promoter of the GPAT and AIRC genes requires binding of Sp1 [33].

To directly characterize the functional interplay between KLF15, NRF-1 and Sp proteins in regulating hPCFT transcription, we used *Drosophila* SL2 cells which do not express Sp factors [34]. A particular goal was to directly assess whether Sp proteins regulate hPCFT promoter activity when all three *cis*-elements (KLF15, GC-Box, and NRF-1) are present, and to determine potential transactivating (or repressive) effects of the broader family of Sp proteins (Sp1, and the short Sp3 and long USp3 isoforms [26,27]) on the hPCFT minimal promoter.

Initially, SL2 cells were transiently transfected with the hPCFT −50/+96 core promoter construct (in pGL3-Basic) and Sp factors (in pPac vector) or empty vector (pPacO). Luciferase assays were performed, with results normalized to the protein levels of each sample. Luciferase activity measured for SL2 cells transfected with the −50/+96 promoter construct and empty vector pPacO was nominal (Figure 4A). Sp1 activated the hPCFT minimal promoter by ~9.4-fold, implicating an important transactivating role for the GC-Box element and Sp1 protein in the absence of other transcription factors (Figure 4A). Compared with Sp1, the USp3 long form transactivated the hPCFT promoter to a lesser extent (~3.4-fold), whereas the shorter Sp3 form [26,27] was even less effective (~1.6-fold) in stimulating reporter gene activity. When combined with Sp1, both USp3 and Sp3 decreased the extent of Sp1 transactivation. Likewise, the Sp3 short form negatively impacted promoter transactivation by its longer Sp3 form (Figure 4A).

Additional experiments further explored the regulation of hPCFT transcription by KLF15 and NRF-1 and the functional relationships between Sp1, KLF15, and NRF-1 in SL2 cells. NRF-1 alone activated the hPCFT core promoter activity by ~43-fold; co-transfection of NRF-1 with Sp factors (Sp1 and Sp3) resulted in modestly decreased (13–42%) promoter activity compared with NRF-1 alone (Figure 4A). Interestingly, KLF15 alone was nominally (~2.3-fold) activating (Figure 4A), but when KLF15 was combined with Sp1 and USp3, promoter activity was stimulated ~16- and 6.2-fold, respectively. Combined NRF-1 and KLF15 transactivated the hPCFT core promoter ~83-fold (Figure 4A), establishing synergistic transactivation by these factors. Promoter activation by combined NRF-1 and KLF15 was decreased by the addition of Sp1 (~20%), USp3 (~27%) or Sp3 (~13%).

To further assess the role of the GC-Box on hPCFT core promoter activity, transactivation by single (Sp1, KLF15 or NRF-1) or combined (KLF15 + Sp1 or NRF-1 + Sp1) transcription

factors was compared for the −50/+96 WT and −50/+96 GC mutant (GC-Boxm) constructs by transient transfections of SL2 cells (Figure 4B). In all cases, compared with the WT promoter construct, promoter activity was lower (~19–43%) for the GC-Box mutant construct, further supporting the notion that transactivation of the hPCFT promoter by these transcription factors is coordinated, as suggested by the results in Figure 4A.

Collectively, these results establish that the hPCFT minimal promoter is regulated in a coordinated fashion by NRF-1, KLF15 and Sp proteins, resulting in both activation and antagonistic responses. Substantial transactivation of hPCFT core promoter activity was achieved by NRF-1 combined with KLF15, in direct support of the notion that these factors are essential to the transcriptional regulation of hPCFT.

Binding of NRF-1, KLF15, and Sp1 transcriptional factors to the hPCFT minimal promoter region

To assess binding of NRF-1, KLF15 and Sp1 proteins to the hPCFT minimal promoter, ChIP assays were performed. Chromatins from HepG2 and HT1080 cells were incubated with IgG (negative control) or ChIP grade NRF-1, KLF15, or Sp1 antibodies. Immunoprecipitated chromatins were amplified by real-time PCR with primers spanning the putative NRF-1 (positions −15 to +1), or the KLF15 (−48 to −29) and GC-Box (−30 to −14) *cis*-elements, to quantitatively assess *in vivo* transcription factor binding.

Whereas NRF-1, KLF15, and Sp1 proteins all significantly bound to the HepG2 chromatin in excess of the negative (IgG) controls, for HT1080 cells divergent results were obtained. Thus, binding of both NRF-1 and Sp1 was detected in HT1080 cells, albeit at ~3-fold and ~2.4-fold lower levels than were recorded for HepG2 cells (Figure 5A). No significant binding of KLF15 in HT1080 cells could be detected over that measured with IgG.

In vitro binding of NRF-1, Sp1 and KLF15 factors to their specific binding sites in the hPCFT promoter was assessed by EMSA. For these experiments, HepG2 and HT1080 NE were incubated with IRDye700-labeled double-strand oligonucleotides, including specific transcription factor binding sequences in the hPCFT promoter. Binding specificities were established by incubations in the presence of excess (200-fold) unlabeled WT or mutant oligonucleotides (see Supplementary Table S3 for the oligonucleotide sequences). DNA–protein complexes were separated on 5% PAGE gels and detected by infrared imaging.

For NRF-1, two specific complexes (a and b) were formed with HepG2 and HT1080 NE which showed modest (~40%) decreases in HT1080 cells (Figure 5B; upper panels). These DNA–protein complexes completely disappeared in the presence of excess untagged NRF-1 oligonucleotide, although the competition was abolished when the NRF-1 core binding sequence was mutated. For DNA/protein complexes formed with HepG2 NE, NRF-1 antibody resulted in a decreased DNA/protein (complex b) signal and two supershifted complexes (labeled 1 and 2). This establishes the specificity of complex formation and identifies the protein complexes as involving NRF-1.

At least five specific DNA–protein complexes (labeled c, d, e, f, and g) were formed upon incubation of IRDye700-labeled KLF15 oligonucleotide with HepG2 NE; these complexes

could be competed away by excess KLF15 WT oligonucleotide but not by KLF15 mutant oligonucleotide (Figure 5B, middle left panel). In HT1080 cells, complexes c, e, f, and g were likewise detected (albeit all at low levels), whereas complex d was undetectable (Figure 5B, middle right panel). DNA/protein complexes formed with HepG2 cells (d, e, f, and g) were supershifted with antibody to KLF15 (labeled 3), establishing specificity.

For Sp1, two major specific DNA–protein complexes (h and i) were detected with significantly higher binding in HepG2 than HT1080 cells (Figure 5B, lower panels). In HepG2 cells, one of two bands comprising complex h (but not complex i) was substantially decreased upon Sp1 antibody treatment (labeled 4 in Figure 5B), confirming Sp1 specificity. However, the identities of the other complex h band or complex i could not be determined on supershifts; these may represent Sp3 protein complexes.

Thus, binding of NRF-1, KLF15, and Sp1 to the hPCFT promoter both *in vivo* (Figure 5A) and in vitro (Figure 5B) paralleled levels of gene expression for these factors (Figure 3A).

As our previous study of Sp1/Sp3 binding to the cystathionine-β-synthetase promoter identified an important role for changes in Sp1/Sp3 phosphorylation in transcription factor binding and gene transactivation in HT1080 cells [35], we hypothesized that a similar mechanism may occur for Sp protein binding to the hPCFT promoter. To assess this possibility, we treated the HT1080 NE with protein kinase A, followed by EMSA (Figure 5C). Binding of Sp factors to the GC-Box sequence was substantially enhanced upon pretreatment with protein kinase A and protein binding was competed by unlabeled WT GC-Box oligonucleotide (Figure 5C). These results strongly suggest that phosphorylation of Sp factors plays an additional important role in their binding to the minimal hPCFT promoter and that decreased Sp protein phosphorylation may further contribute to the modest hPCFT promoter activity and low levels of hPCFT measured in HT1080 cells.

Expression and regulatory associations between hPCFT and NRF-1, Sp1, or KLF15 in human solid tumor cell lines

Interestingly, when NRF-1 or Sp1 and hPCFT transcripts were measured in a cohort of 53 human solid tumor cell lines previously reported with wide-ranging hPCFT levels [3] (Supplementary Table S4), close associations were detected between NRF-1 and hPCFT (r = 0.4016 and p = 0.0029 by Pearson's correlation; Figure 6A) and between Sp1 and hPCFT (r = 0.4165 and p = 0.0019; Figure 6B). However, this association was less exact between KLF15 and hPCFT (r = 0.1288 and p = 0.3579; Figure 6C). To assess whether these associations could be direct or indirect, the MRNETB method with Pearson's correlations was used [28,29]. This multivariate regulatory inference analysis showed direct associations between the hPCFT and each factor (NRF-1, Sp1, or KLF15). In the schematic (Figure 6D), the degree of association was different for different transcription factors, with stronger associations between hPCFT and NRF-1 or Sp1 than with KLF15.

Discussion

We discovered novel 6-substituted pyrrolo[2,3-*d*]pyrimidine antifolates typified by AGF94 with substantial selectivity for hPCFT over the reduced folate carrier (the major tissue folate

transporter), resulting in potent anti-tumor efficacy *in vitro* and *in vivo* [6,17,18,36,37]. While the development of hPCFT-targeted therapies is based on the notion that hPCFT is highly expressed in human tumors, the reality among assorted human tumor cell lines and primary tumors (including NSCLC, malignant pleural mesothelioma, and epithelial ovarian cancer) is that both high- and low-expressing cases are detected [3–6]. Given the importance of understanding the regulation of hPCFT to the effective implementation of hPCFT-targeted therapies for cancer, characterization of the underlying mechanisms that contribute to these variations in hPCFT gene expression is essential.

In this report, we investigated the basis for differences in sensitivities for HepG2 and HT1080 tumor cells to AGF94, a prototypical hPCFT-selective antifolate [18]. Loss of AGF94 sensitivity in HT1080 cells was associated with negligible levels of hPCFT transcripts and protein, whereas HepG2 cells expressed elevated hPCFT. The lack of detectable hPCFT in HT1080 cells was not due to the loss of hPCFT alleles or to alterations in the hPCFT promoter sequence. Furthermore, treatment with 5-Aza and bisulfite DNA sequencing suggested that loss of hPCFT gene expression in HT1080 cells did not result from CpG hypermethylation in the hPCFT promoter. Rather, reporter assays with hPCFT promoter constructs (−2005/+96 to −35/+96) suggested that, most likely, the disparate levels of hPCFT levels in HepG2 and HT1080 cells reflected differences in critical transcriptional controls.

Our analysis localized a core hPCFT promoter to between positions −50 and +96, including KLF15, GC-Box, and NRF-1 *cis*-elements. The functional importance of these elements was verified by mutation of core consensus sequences, transient transfections with expression constructs for the transcription factors, and reporter gene assays in HepG2, HT1080, and *Drosophila* SL2 cells. Substantial and synergistic transactivation of hPCFT core promoter activity was achieved by NRF-1 combined with KLF15. While KLF15 and Sp1 were cooperative in activating hPCFT, Sp3 proteins were distinctly antagonistic. NRF-1 and Sp1 were also antagonistic, a pattern that continued with both the short and long Sp3 protein forms [27]. Binding of NRF-1, Sp1, and KLF15 to the endogenous hPCFT promoter in HepG2 and HT1080 cells was confirmed by ChIP analysis and was further validated *in vitro* by EMSA and supershifts. The results of both these assays were highly concordant, and the stoichiometries of NRF-1, KLF15 and Sp1 binding to the hPCFT promoter in HepG2 and HT1080 cells paralleled the expression levels of these transcription factors. Collectively, these results establish the transcriptional potentials of NRF-1, KLF15 and Sp proteins in regulating hPCFT transcription. While NRF-1 was previously reported to regulate hPCFT via binding to the hPCFT core promoter [13], our results are the first to identify an important role for KLF15 in regulating hPCFT gene expression. To the best of our knowledge, functional cooperativity between NRF-1 and KLF15 in gene transactivation has not been previously reported.

KLF15 is involved in assorted biological processes, including cell proliferation, differentiation, and death. KLF15 regulates its transcriptional targets in cardiac metabolism via interaction with p300 and recruitment of this critical co-activator to promoters [38]. KLF15 is a regulator of adipogenesis [39] and is a central component of the transcriptional circuitry that regulates physiologic fluxes of all three major nutrient classes (i.e. glucose,

lipids, and amino acids) [40,41]. Our present results now extend the metabolic scope of KLF15 to include one-carbon homeostasis, via its transcriptional regulation of hPCFT, a critical route for intestinal uptake of folates [1,42]. Both KLF15 and hPCFT are highly expressed in kidney, liver, placenta and small intestine [1,36,39,42,43]. KLF15 has been implicated in the development of human malignancies, including breast cancer for which it plays a role as a novel tumor suppressor [44]. The *EWSR1–KLF15* fusion transcript is associated with primary renal myoepithelial carcinoma in children [45]. Our finding of a critical role of KLF15 in hPCFT gene expression is intriguing given the demonstrated cooperativity of KLF15 with the glucocorticoid receptor in regulating genes involved in amino acid metabolism [46]. By analogy, the previously observed regulation of hPCFT by the glucocorticoid receptor [47] may also be mediated via KLF15.

The NRF-1-binding motif is frequently found in a large number of TATA-less promoters near the transcriptional start site, and it has been suggested that NRF-1 plays a major role as a proximal promoter-binding factor [48]. NRF-1 has been identified as a transcriptional regulator of genes involved in mitochondrial biogenesis [49] and also plays a role in regulating and coordinating assorted genes involved in embryonic development [50], cell proliferation, and DNA synthesis and repair [51,52]. NRF-1 expression is selectively up-regulated in human breast cancer cells relative to adjacent stromal tissue, which correlates with metastasis and poor prognosis [53]. Finally, the up-regulation of NRF-1 is observed in type I endometrial cancer [54] and thyroid oncocytoma [55].

Sp proteins regulate a vast array of genes involved in essential cellular functions, including proliferation, differentiation, DNA damage response, apoptosis, senescence and angiogenesis [26,27]. Whereas Sp1 is typically an activator of transcription, Sp3 exerts both agonistic and antagonistic effects on gene expression [26,27]. Consistent with our findings for hPCFT, KLF15 and Sp1 cooperate in regulating gene expression [31,32] via stable interaction between these factors [32]. NRF-1 binding to the GPAT and AIRC shared promoter also requires Sp1 [33].

hPCFT is expressed in human tumor cell lines from a variety of lineages [3–6] and the results described herein are best interpreted in terms of a highly coordinate regulation of hPCFT gene expression by KLF15, NRF-1, and Sp1. Although overexpression of NRF-1, KLF15, and Sp1 significantly impacted hPCFT expression in HepG2 cells, there was no impact in HT1080 cells. While excellent associations were established between the expression of NRF-1 or Sp1 and hPCFT among a cohort of 53 human tumor cell lines, this was slightly reduced for KLF15 and hPCFT. Thus, levels of NRF-1 and Sp1, and to a lesser extent KLF15, appear to be critical determinants of hPCFT gene expression in a broad range of human tumor cells. Of course, the functions of these factors in regulating hPCFT transcription are also regulated by their posttranslational modifications [56,57] or via associations with other transcription factors [58] not considered herein. Consistent with the former, protein kinase A treatment of HT1080 NE significantly increased Sp1 binding to the hPCFT promoter by EMSA, suggesting an additional potential role of Sp1 phosphorylation in regulating hPCFT transcription.

In conclusion, we have identified critical transcription factors including KLF15, NRF-1, and Sp1/Sp3 that regulate the hPCFT minimal promoter. Our results suggest that alterations in the levels of KLF15 and NRF-1 are likely causal in the low levels of hPCFT in HT1080 cells and possibly other low hPCFT-expressing tumors and that levels and function of these critical factors may be important determinants of hPCFT expression and anti-tumor efficacy of hPCFT-targeted agents such as AGF94. Additional roles of posttranslational modifications of critical factors, as suggested for Sp1, may manifest. Compelling preclinical evidence suggests the extraordinary therapeutic potential of hPCFT-targeted cytotoxic drugs for cancer [17] which would be further enhanced if strategies can be developed for selectively increasing hPCFT expression and/or transport activity.

Supplementary Material

Refer to Web version on PubMed Central for supplementary material.

Funding

This study was supported by grants R01 CA53535 (L.H.M. and Z.H.), R01 CA152316 (L.H.M. and A.G.), and R01 CA166711 (A.G. and L.H.M.) from the National Cancer Institute, the Eunice and Milton Ring Endowed Chair for Cancer Research (L.H.M.), and the Duquesne University Adrian Van Kaam Chair in Scholarly Excellence (A.G.). The Biostatistics Core of the Barbara Ann Karmanos Cancer Institute (S.K.) was supported, in part, by NIH Center grant P30 CA022453 to the Karmanos Cancer Institute and the Wayne State University.

Abbreviations

5-Aza	5-aza-2′deoxycytidine
ChIP	chromatin immunoprecipitation
EMSA	electrophoretic mobility shift assay
GAPDH	glyceraldehyde-3-phosphate dehydrogenase
hPCFT	human PCFT
KLF15	Krüppel-like factor 15
MRNETB	maximum relevance minimum redundancy backward
MTX	methotrexate
NE	nuclear extract
NRF-1	nuclear respiratory factor-1
NSCLC	non-small cell lung cancer
PCFT	proton-coupled folate transporter
PMX	pemetrexed
Sp	stimulatory protein
WT	wild-type

References

1. Qiu A, Jansen M, Sakaris A, Min SH, Chattopadhyay S, Tsai E et al. (2006) Identification of an intestinal folate transporter and the molecular basis for hereditary folate malabsorption. Cell 127, 917–928 10.1016/j.cell.2006.09.041 [PubMed: 17129779]
2. Zhao R, Aluri S and Goldman ID (2017) The proton-coupled folate transporter (PCFT-SLC46A1) and the syndrome of systemic and cerebral folate deficiency of infancy: hereditary folate malabsorption. Mol. Aspects Med. 53, 57–72 10.1016/j.mam.2016.09.002 [PubMed: 27664775]
3. Desmoulin SK, Wang L, Hales E, Polin L, White K, Kushner J et al. (2011) Therapeutic targeting of a novel 6-substituted pyrrolo [2,3-d] pyrimidine thienoyl antifolate to human solid tumors based on selective uptake by the proton-coupled folate transporter. Mol. Pharmacol 80, 1096–1107 10.1124/mol.111.073833 [PubMed: 21940787]
4. Giovannetti E, Zucali PA, Assaraf YG, Funel N, Gemelli M, Stark M et al. (2017) Role of proton-coupled folate transporter in pemetrexed-resistance of mesothelioma: clinical evidence and new pharmacological tools. Ann. Oncol 28, 2725–2732 10.1093/annonc/mdx499 [PubMed: 28945836]
5. Hou Z, Gattoc L, O'Connor C, Yang S, Wallace-Povirk A, George C et al. (2017) Dual targeting of epithelial ovarian cancer via folate receptor α and the proton-coupled folate transporter with 6-substituted pyrrolo[2,3-*d*]pyrimidine antifolates. Mol. Cancer Ther. 16, 819–830 10.1158/1535-7163.MCT-16-0444 [PubMed: 28138029]
6. Wilson MR, Hou Z, Yang S, Polin L, Kushner J, White K et al. (2016) Targeting nonsquamous nonsmall cell lung cancer via the proton-coupled folate transporter with 6-substituted pyrrolo[2,3-*d*]pyrimidine thienoyl antifolates. Mol. Pharmacol 89, 425–434 10.1124/mol.115.102798 [PubMed: 26837243]
7. Gonen N, Bram EE and Assaraf YG (2008) PCFT/SLC46A1 promoter methylation and restoration of gene expression in human leukemia cells. Biochem. Biophys. Res. Commun 376, 787–792 10.1016/j.bbrc.2008.09.074 [PubMed: 18817749]
8. Zhao R and Goldman ID (2007) The molecular identity and characterization of a proton-coupled folate transporter – PCFT; biological ramifications and impact on the activity of pemetrexed. Cancer Metastasis Rev. 26, 129–139 10.1007/s10555-007-9047-1 [PubMed: 17340171]
9. Zhao R, Qiu A, Tsai E, Jansen M, Akabas MH and Goldman ID (2008) The proton-coupled folate transporter: impact on pemetrexed transport and on antifolates activities compared with the reduced folate carrier. Mol. Pharmacol 74, 854–862 10.1124/mol.108.045443 [PubMed: 18524888]
10. Hazarika M, White RM, Johnson JR and Pazdur R (2004) FDA drug approval summaries: pemetrexed (Alimta). Oncologist 9, 482–488 10.1634/theoncologist.9-5-482 [PubMed: 15477632]
11. Cohen MH, Justice R and Pazdur R (2009) Approval summary: pemetrexed in the initial treatment of advanced/metastatic non-small cell lung cancer. Oncologist 14, 930–935 10.1634/theoncologist.2009-0092 [PubMed: 19737998]
12. Diop-Bove NK, Wu J, Zhao R, Locker J and Goldman ID (2009) Hypermethylation of the human proton-coupled folate transporter (SLC46A1) minimal transcriptional regulatory region in an antifolate-resistant HeLa cell line. Mol. Cancer Ther. 8, 2424–2431 10.1158/1535-7163.MCT-08-0938 [PubMed: 19671745]
13. Gonen N and Assaraf YG (2010) The obligatory intestinal folate transporter PCFT (SLC46A1) is regulated by nuclear respiratory factor 1. J. Biol. Chem 285, 33602–33613 10.1074/jbc.M110.135640 [PubMed: 20724482]
14. Stark M, Gonen N and Assaraf YG (2009) Functional elements in the minimal promoter of the human proton-coupled folate transporter. Biochem. Biophys. Res. Commun 388, 79–85 10.1016/j.bbrc.2009.07.116 [PubMed: 19643086]
15. Furumiya M, Inoue K, Ohta K, Hayashi Y and Yuasa H (2013) Transcriptional regulation of PCFT by KLF4, HNF4alpha, CDX2 and C/EBPalpha: Implication in its site-specific expression in the small intestine. Biochem. Biophys. Res. Commun 431, 158–163 10.1016/j.bbrc.2013.01.004 [PubMed: 23313509]
16. Eloranta JJ, Zair ZM, Hiller C, Hausler S, Stieger B and Kullak-Ublick GA (2009) Vitamin D3 and its nuclear receptor increase the expression and activity of the human proton-coupled folate transporter. Mol. Pharmacol 76, 1062–1071 10.1124/mol.109.055392 [PubMed: 19666701]

17. Matherly LH, Hou Z and Gangjee A (2018) The promise and challenges of exploiting the proton-coupled folate transporter for selective therapeutic targeting of cancer. Cancer Chemother. Pharmacol 81, 1–15 10.1007/s00280-017-3473-8 [PubMed: 29127457]
18. Wang L, Desmoulin SK, Cherian C, Polin L, White K, Kushner J et al. (2011) Synthesis, biological, and antitumor activity of a highly potent 6-substituted pyrrolo[2,3-*d*]pyrimidine thienoyl antifolate inhibitor with proton-coupled folate transporter and folate receptor selectivity over the reduced folate carrier that inhibits β-glycinamide ribonucleotide formyltransferase. J. Med. Chem 54, 7150–7164 10.1021/jm200739e [PubMed: 21879757]
19. Otteson DC, Liu Y, Lai H, Wang C, Gray S, Jain MK et al. (2004) Krüppel-like factor 15, a zinc-finger transcriptional regulator, represses the rhodopsin and interphotoreceptor retinoid-binding protein promoters. Invest. Ophthalmol. Vis. Sci 45, 2522–2530 10.1167/iovs.04-0072 [PubMed: 15277472]
20. Desmoulin SK, Wang Y, Wu J, Stout M, Hou Z, Fulterer A et al. (2010) Targeting the proton-coupled folate transporter for selective delivery of 6-substituted pyrrolo[2,3-d]pyrimidine antifolate inhibitors of de novo purine biosynthesis in the chemotherapy of solid tumors. Mol. Pharmacol 78, 577–587 10.1124/mol.110.065896 [PubMed: 20601456]
21. Wilson MR, Hou Z and Matherly LH (2014) Substituted cysteine accessibility reveals a novel transmembrane 2–3 reentrant loop and functional role for transmembrane domain 2 in the human proton-coupled folate transporter. J. Biol. Chem 289, 25287–25295 10.1074/jbc.M114.578252 [PubMed: 25053408]
22. Laemmli UK (1970) Cleavage of structural proteins during the assembly of the head of bacteriophage T4. Nature 227, 680–685 10.1038/227680a0 [PubMed: 5432063]
23. Matsudaira P (1987) Sequence from picomole quantities of proteins electroblotted onto polyvinylidene difluoride membranes. J. Biol. Chem 262, 10035–10038 [PubMed: 3611052]
24. Hou Z, Kugel Desmoulin S, Etnyre E, Olive M, Hsiung B, Cherian C et al. (2012) Identification and functional impact of homo-oligomers of the human proton-coupled folate transporter. J. Biol. Chem 287, 4982–4995 10.1074/jbc.M111.306860 [PubMed: 22179615]
25. Lowry OH, Rosebrough NJ, Farr AL and Randall RJ (1951) Protein measurement with the Folin phenol reagent. J. Biol. Chem 193, 265–275 [PubMed: 14907713]
26. Beishline K and Azizkhan-Clifford J (2015) Sp1 and the 'hallmarks of cancer'. FEBS J. 282, 224–258 10.1111/febs.13148 [PubMed: 25393971]
27. Suske G (1999) The Sp-family of transcription factors. Gene 238, 291–300 10.1016/S0378-1119(99)00357-1 [PubMed: 10570957]
28. Meyer PE, Lafitte F and Bontempi G (2008) minet: a R/Bioconductor package for inferring large transcriptional networks using mutual information. BMC Bioinformatics 9, 461 10.1186/1471-2105-9-461 [PubMed: 18959772]
29. Meyer P, Marbach D, Roy S and Kellis M (2010) Information-theoretic inference of gene networks using backward elimination. BioComp. 700–705
30. Cartharius K, Frech K, Grote K, Klocke B, Haltmeier M, Klingenhoff A et al. (2005) MatInspector and beyond: promoter analysis based on transcription factor binding sites. Bioinformatics 21, 2933–2942 10.1093/bioinformatics/bti473 [PubMed: 15860560]
31. Li J, Yang Y, Jiang B, Zhang X, Zou Y and Gong Y (2010) Sp1 and KLF15 regulate basal transcription of the human LRP5 gene. BMC Genet. 11, 12 10.1186/1471-2156-11-12 [PubMed: 20141633]
32. Yamamoto J, Ikeda Y, Iguchi H, Fujino T, Tanaka T, Asaba H et al. (2004) A Krüppel-like factor KLF15 contributes fasting-induced transcriptional activation of mitochondrial acetyl-CoA synthetase gene AceCS2. J. Biol. Chem 279, 16954–16962 10.1074/jbc.M312079200 [PubMed: 14960588]
33. Chen S, Nagy PL and Zalkin H (1997) Role of NRF-1 in bidirectional transcription of the human GPAT-AIRC purine biosynthesis locus. Nucleic Acids Res. 25, 1809–1816 10.1093/nar/25.9.1809 [PubMed: 9108165]
34. Pascal E and Tjian R (1991) Different activation domains of Sp1 govern formation of multimers and mediate transcriptional synergism. Genes Dev. 5, 1646–1656 10.1101/gad.5.9.1646 [PubMed: 1885006]

35. Ge Y, Matherly LH and Taub JW (2001) Transcriptional regulation of cell-specific expression of the human cystathionine β-synthase gene by differential binding of Sp1/Sp3 to the −1b promoter. J. Biol. Chem 276, 43570–43579 10.1074/jbc.M104930200 [PubMed: 11562358]
36. Desmoulin SK, Hou Z, Gangjee A and Matherly LH (2012) The human proton-coupled folate transporter: biology and therapeutic applications to cancer. Cancer Biol. Ther 13, 1355–1373 10.4161/cbt.22020 [PubMed: 22954694]
37. Wang L, Wallace A, Raghavan S, Deis SM, Wilson MR, Yang S et al. (2015) 6-Substituted pyrrolo[2,3-d]pyrimidine thienoyl regioisomers as targeted antifolates for folate receptor α and the proton-coupled folate transporter in human tumors. J. Med. Chem 58, 6938–6959 10.1021/acs.jmedchem.5b00801 [PubMed: 26317331]
38. Prosdocimo DA, Anand P, Liao X, Zhu H, Shelkay S, Artero-Calderon P et al. (2014) Krü-like factor 15 is a critical regulator of cardiac lipid metabolism. J. Biol. Chem 289, 5914–5924 10.1074/jbc.M113.531384 [PubMed: 24407292]
39. Gray S, Feinberg MW, Hull S, Kuo CT, Watanabe M, Sen-Banerjee S et al. (2002) The Krüppel-like factor KLF15 regulates the insulin-sensitive glucose transporter GLUT4. J. Biol. Chem 277, 34322–34328 10.1074/jbc.M201304200 [PubMed: 12097321]
40. Gray S, Wang B, Orihuela Y, Hong EG Fisch S, Haldar S et al. (2007) Regulation of gluconeogenesis by Krüppel-like factor 15. Cell Metab. 5, 305–312 10.1016/j.cmet.2007.03.002 [PubMed: 17403374]
41. Haldar SM, Jeyaraj D, Anand P, Zhu H, Lu Y, Prosdocimo DA et al. (2012) Krüppel-like factor 15 regulates skeletal muscle lipid flux and exercise adaptation. Proc. Natl Acad. Sci. U.S.A. 109, 6739–6744 10.1073/pnas.1121060109 [PubMed: 22493257]
42. Zhao R, Matherly LH and Goldman ID (2009) Membrane transporters and folate homeostasis: intestinal absorption and transport into systemic compartments and tissues. Exp. Rev. Mol. Med 11, e4 10.1017/S1462399409000969
43. Uchida S, Tanaka Y, Ito H, Saitoh-Ohara F, Inazawa J, Yokoyama KK et al. (2000) Transcriptional regulation of the CLC-K1 promoter by myc-associated zinc finger protein and kidney-enriched Krüppel-like factor, a novel zinc finger repressor. Mol. Cell. Biol 20, 7319–7331 10.1128/MCB.20.19.7319-7331.2000 [PubMed: 10982849]
44. Yoda T, McNamara KM, Miki Y, Onodera Y, Takagi K, Nakamura Y et al. (2015) KLF15 in breast cancer: a novel tumor suppressor? Cell. Oncol 38, 227–235 10.1007/s13402-015-0226-8
45. Cajaiba MM, Jennings LJ, Rohan SM, Leuer KM, Anagnost MR, Fahner JB et al. (2016) Expanding the spectrum of renal tumors in children: primary renal myoepithelial carcinomas with a novel EWSR1-KLF15 fusion. Am. J. Surg. Pathol 40, 386–394 10.1097/PAS.0000000000000545 [PubMed: 26523541]
46. Sasse SK, Mailloux CM, Barczak AJ, Wang Q, Altonsy MO, Jain MK et al. (2013) The glucocorticoid receptor and KLF15 regulate gene expression dynamics and integrate signals through feed-forward circuitry. Mol. Cell. Biol 33, 2104–2115 10.1128/MCB.01474-12 [PubMed: 23508109]
47. Patki M, Gadgeel S, Huang Y, McFall T, Shields AF, Matherly LH et al. (2014) Glucocorticoid receptor status is a principal determinant of variability in the sensitivity of non-small-cell lung cancer cells to pemetrexed. J. Thorac. Oncol 9, 519–526 10.1097/JTO.0000000000000111 [PubMed: 24736075]
48. FitzGerald PC, Shlyakhtenko A, Mir AA and Vinson C (2004) Clustering of DNA sequences in human promoters. Genome Res. 14, 1562–1574 10.1101/gr.1953904 [PubMed: 15256515]
49. Evans MJ and Scarpulla RC (1990) NRF-1: a trans-activator of nuclear-encoded respiratory genes in animal cells. Genes & development 4, 1023–1034 10.1101/gad.4.6.1023 [PubMed: 2166701]
50. Huo L and Scarpulla RC (2001) Mitochondrial DNA instability and peri-implantation lethality associated with targeted disruption of nuclear respiratory factor 1 in mice. Mol. Cell. Biol 21, 644–654 10.1128/MCB.21.2.644-654.2001 [PubMed: 11134350]
51. Satoh J, Kawana N and Yamamoto Y (2013) Pathway analysis of ChIP-Seq-based NRF1 target genes suggests a logical hypothesis of their involvement in the pathogenesis of neurodegenerative diseases. Gene Regul. Syst. Biol 7, 139–152 10.4137/GRSB.S13204

52. Scarpulla RC (2008) Transcriptional paradigms in mammalian mitochondrial biogenesis and function. Physiol. Rev 88, 611–638 10.1152/physrev.00025.2007 [PubMed: 18391175]

53. Ertel A, Tsirigos A, Whitaker-Menezes D, Birbe RC, Pavlides S, Martinez-Outschoorn UE et al. (2012) Is cancer a metabolic rebellion against host aging? In the quest for immortality, tumor cells try to save themselves by boosting mitochondrial metabolism. Cell Cycle 11, 253–263 10.4161/cc.11.2.19006 [PubMed: 22234241]

54. Cormio A, Guerra F, Cormio G, Pesce V, Fracasso F, Loizzi V et al. (2009) The PGC-1α-dependent pathway of mitochondrial biogenesis is upregulated in type I endometrial cancer. Biochem. Biophys. Res. Commun 390, 1182–1185 10.1016/j.bbrc.2009.10.114 [PubMed: 19861117]

55. Savagner F, Mirebeau D, Jacques C, Guyetant S, Morgan C, Franc B et al. (2003) PGC-1-related coactivator and targets are upregulated in thyroid oncocytoma. Biochem. Biophys. Res. Commun 310, 779–784 10.1016/j.bbrc.2003.09.076 [PubMed: 14550271]

56. Gugneja S and Scarpulla RC (1997) Serine phosphorylation within a concise amino-terminal domain in nuclear respiratory factor 1 enhances DNA binding. J. Biol. Chem 272, 18732–18739 10.1074/jbc.272.30.18732 [PubMed: 9228045]

57. Tan NY and Khachigian LM (2009) Sp1 phosphorylation and its regulation of gene transcription. Mol. Cell. Biol 29, 2483–2488 10.1128/MCB.01828-08 [PubMed: 19273606]

58. McConnell BB and Yang VW (2010) Mammalian Krüppel-like factors in health and diseases. Physiol. Rev 90, 1337–1381 10.1152/physrev.00058.2009 [PubMed: 20959618]

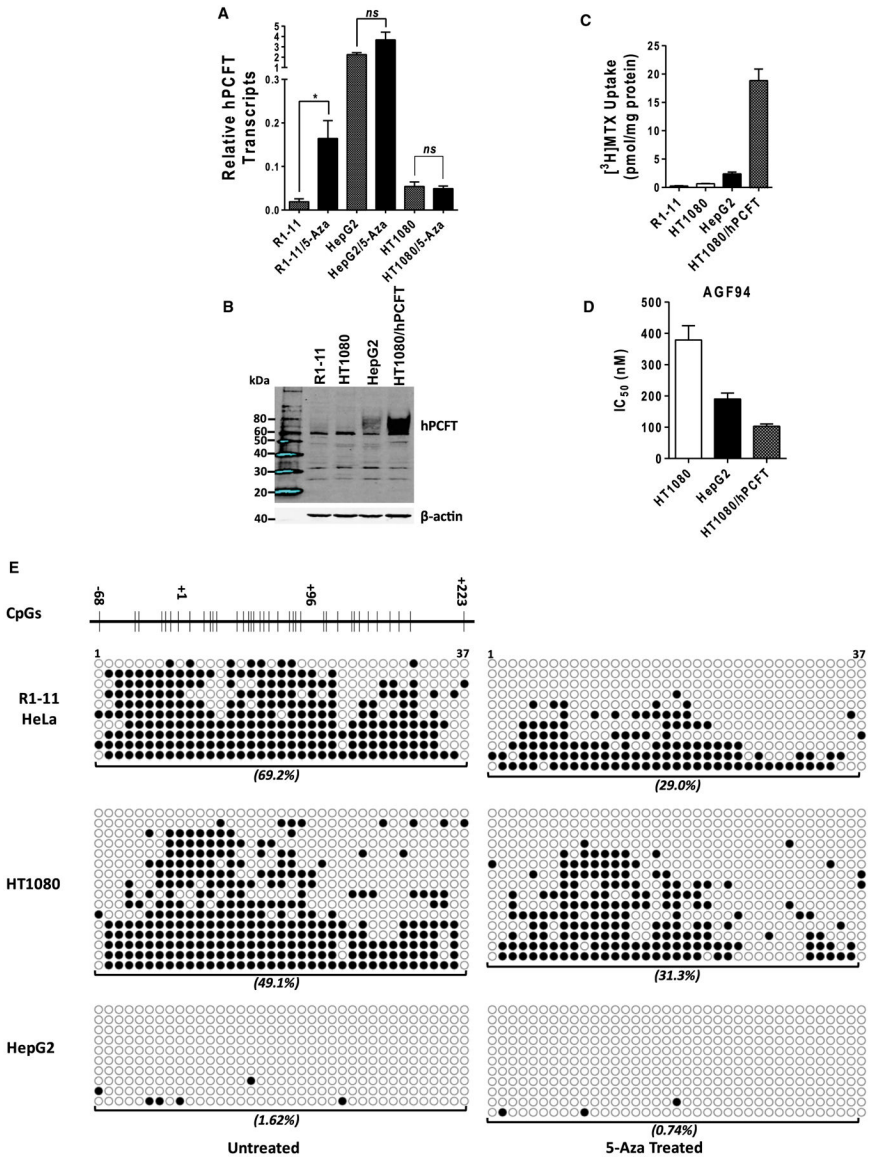

Figure 1. Transcriptional regulation of hPCFT gene expression.

(**A**) R1–11 HeLa, HT1080 and HepG2 cells were plated and treated with 2 μM 5-Aza or DMSO (vehicle) for 72 h. The cells were harvested for RNA extraction for hPCFT gene expression analysis by real-time RT-PCR with a LightCycler 480 Probes Master kit. Results are shown as mean values ± standard errors ($n = 3$). *$p < 0.05$; ns, non-significant. (**B**) hPCFT protein levels were measured in crude plasma membranes by SDS–PAGE and Western blotting with hPCFT polyclonal antibody. (**C**) hPCFT uptake was measured with [^{3}H]MTX at pH 5.5 at 37°C for 5 min. Results were calculated as pmol [^{3}H]MTX/mg protein and are shown as mean values ± standard errors ($n = 3$). (**D**) Cells were plated with a range of concentrations of AGF94. Cell proliferation was assayed with CellTiter-Blue and a fluorescent plate reader. Results for drug treatments were normalized to relative growth in the absence of drug additions. Results are shown as mean IC_{50} values (in units of nM) with standard errors ($n = 3$). (**E**) Genomic DNAs (2 μg) from R1–11, HT1080 and HepG2 cells

treated with or without 5-Aza were used for bisulfite conversion. The converted DNAs were used as templates for PCR amplification of a region of the hPCFT promoter (positions −74 to +229) that was reported as heavily methylated [4,7,12]. The amplicons (302 bp) were resolved, gel purified and cloned into pCRII-TOPO vector. Bacteria were transformed and plasmid DNAs from 10 to 16 bacterial clones were prepared for Sanger DNA sequencing. The sequencing results were compared with hPCFT genomic sequence to reveal 37 putative CpGs between positions −74 and +229. The schematic shows the total bacterial clones that were sequenced and the number of methylated CpGs (dark circles) from the 37 CpGs. The percentages of methylated CpGs were calculated and are noted in parentheses.

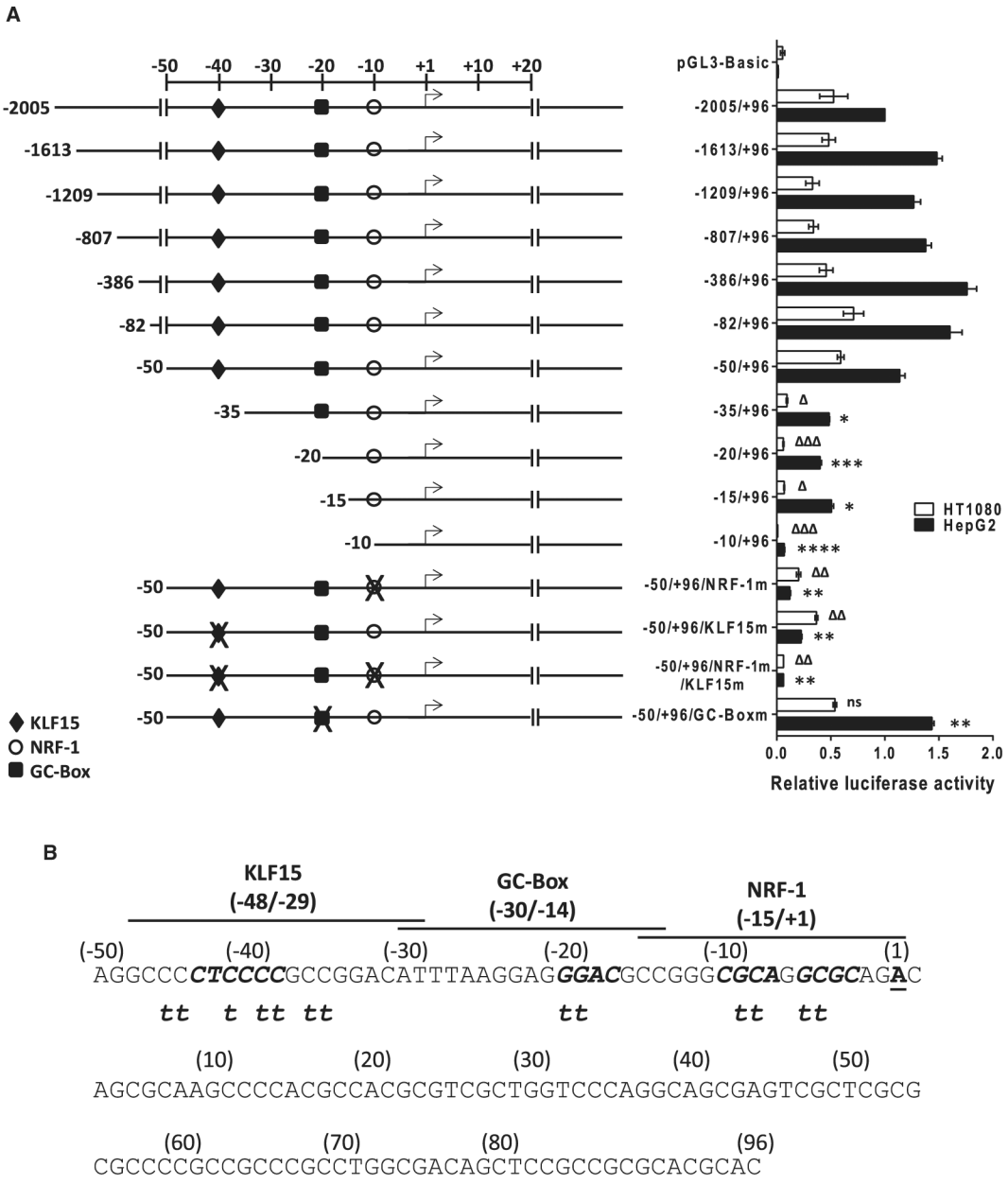

Figure 2. Functional analysis of hPCFT promoter–reporter constructs in HepG2 and HT1080 cells.

(**A**) HT1080 and HepG2 cells were transfected with the full-length (−2005/+96) and progressive deletion (−1613/+96, −1209/+96, −807/+96, −386/+96, −82/+96, −50/+96, −35/+96, −20/+96, −15/+96, −10/+96) constructs, as well as NRF-1, KLF15, or GC-Box consensus mutant constructs in −50/+96 (−50/+96/NRF-1m, −50/+96/KLF15m, −50/+96/NRF-1m/KLF15m, −50/+96/GC-Boxm, respectively). Luciferase activities for the reporter constructs were normalized to Renilla luciferase activities and compared with that of the −50/+96 hPCFT core promoter construct. Data are presented as the mean values ± standard errors from three to seven independent experiments. Statistical analyses for comparisons of luciferase activities for the −50/+96 construct and its deletion and mutation constructs were

performed and are noted. **** or ΔΔΔΔ, $p < 0.0001$; *** or ΔΔΔ, $p < 0.001$; ** or ΔΔ, $p < 0.05$; ns, not significant. (**B**) Bioinformatics analysis was performed using MatInspector [30] and revealed three transcription binding sites from positions −50 to +1 within the hPCFT core promoter (−50/+96) region, including one KLF15, one GC-Box, and one NRF-1 *cis*-element. The core consensus sequences for each element are in bold and are italicized. Below particular bases are shown 't', indicating specific mutations introduced in reporter gene constructs and oligonucleotides used in EMSA to disrupt the *cis*-elements.

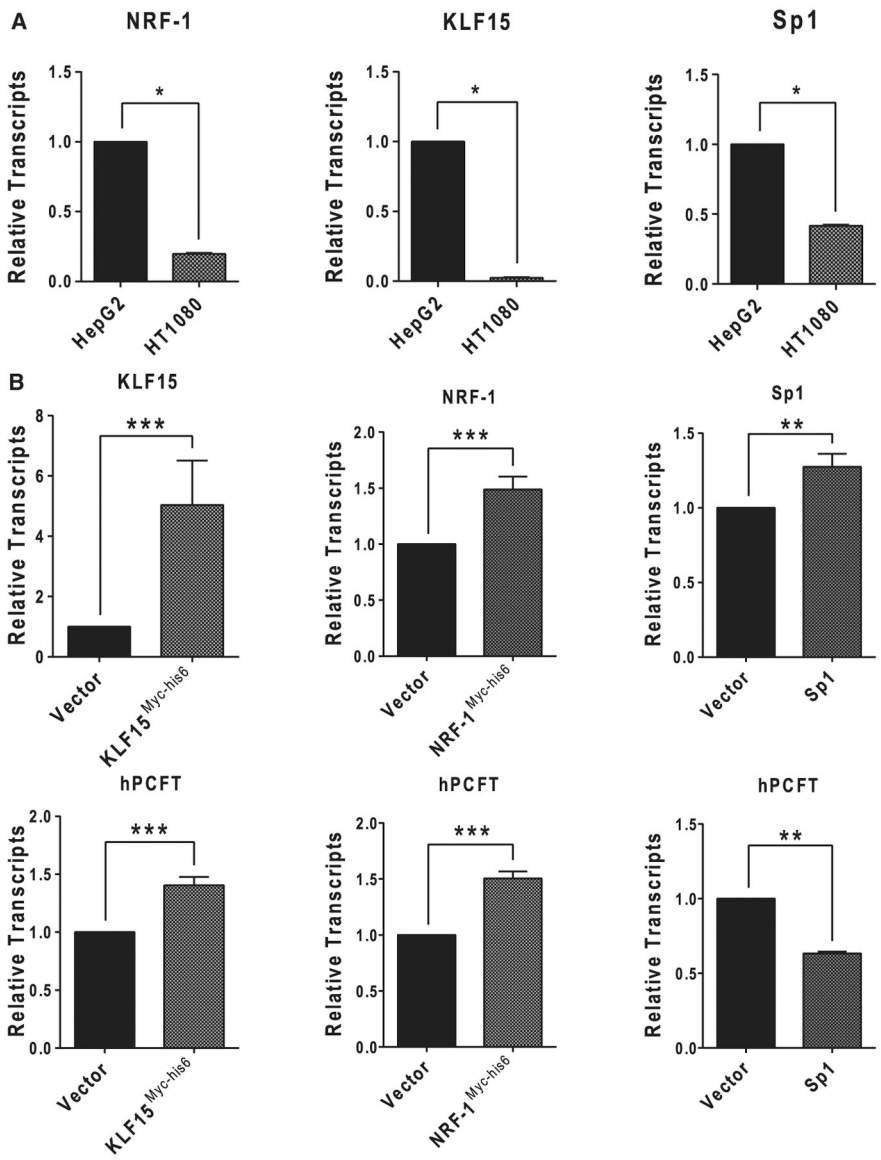

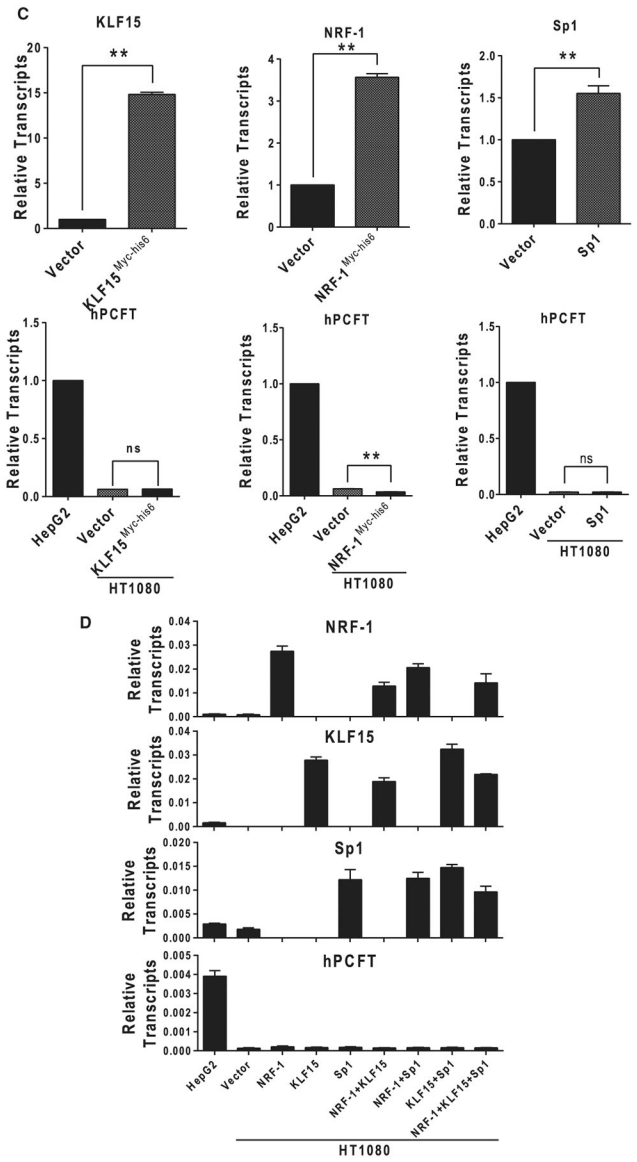

Figure 3. NRF-1, KLF15, and Sp1 expression in HepG2 and HT1080 cells and the impact of NRF-1, KLF15 and Sp1 on hPCFT gene expression.

(**A**) Transcript levels for KLF15, NRF-1 and Sp1 were measured in HepG2 and HT1080 cell lines. (**B**) Impact of hPCFT gene expression in HepG2 cells stably transfected with KLF15, NRF-1 or Sp1. (**C**) Impact of hPCFT gene expression in HT1080 cells stably transfected with KLF15, NRF-1 or Sp1. (**D**) Impact of hPCFT gene expression in HT1080 cells transiently transfected with KLF15, NRF-1 or Sp1 singly or in combination. Transcript levels of NRF-1, KLF15, Sp1 and hPCFT were monitored by real-time RT-PCR with a LightCycler 480 Probes Master kit, or with a LightCycler 480 SYBR Green I Master kit. The transcript levels were normalized to that for GAPDH and/or β-actin. Results are presented as mean values ± standard errors from three to four different experiments. For statistics: ***$p < 0.001$; **$p < 0.01$; *$p < 0.05$.

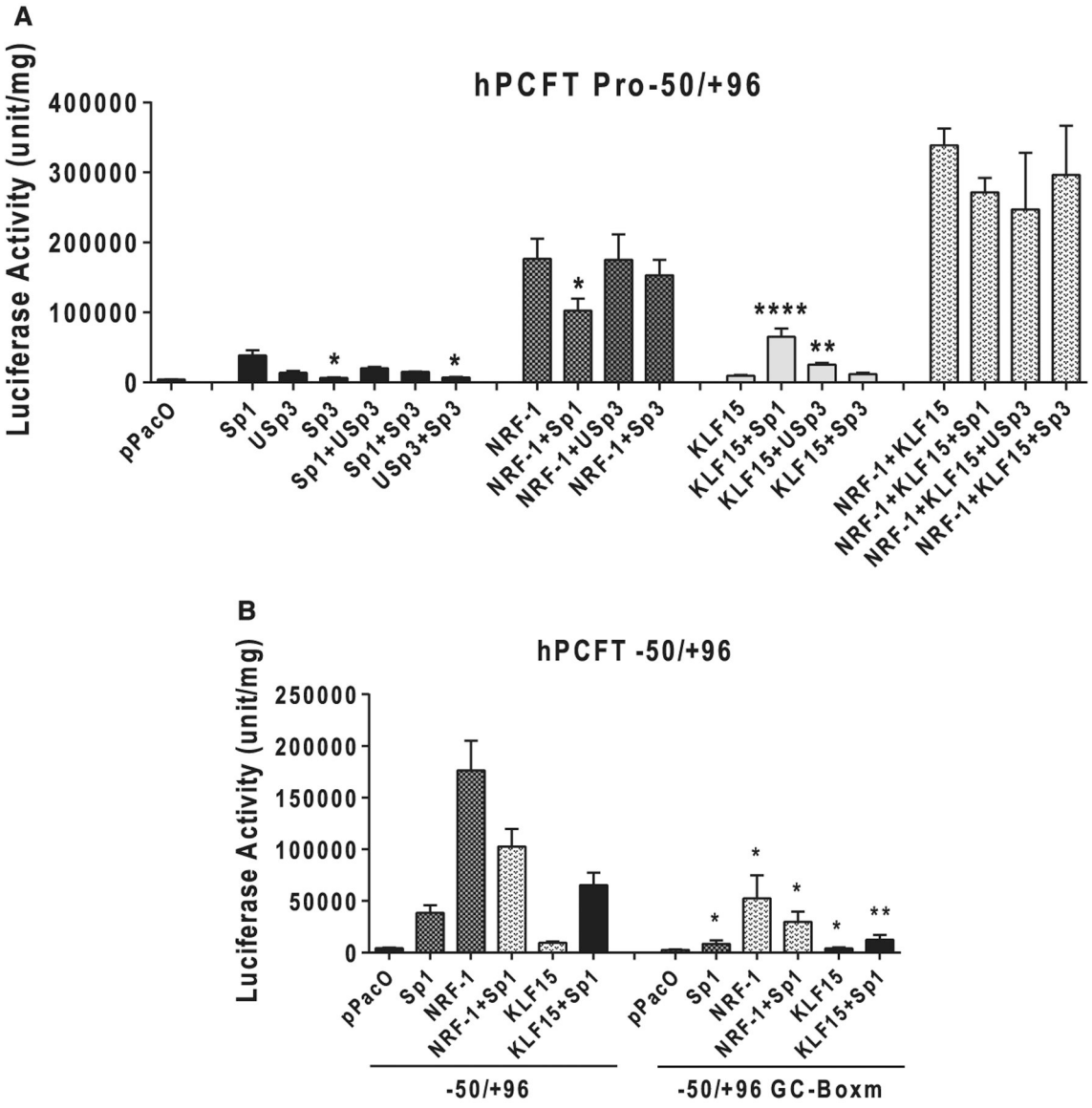

Figure 4. Functional analysis of hPCFT core promoter elements and transcription factors in *Drosophila* SL2 cells.

Drosophila SL2 cells were co-transfected with hPCFT core promoter-luciferase reporter gene constructs −50/+96 and pPacO, or Sp1, USp3 (Sp3 longer form), Sp3 (Sp3 shorter form), NRF-1, or KLF15 cDNA constructs in pPacO using FuGENE 6 transfection reagent. Cells were harvested after 48 h for luciferase assays using a single-luciferase assay system with a microplate reader. Luciferase activities were normalized to cell proteins. (**A**) Effects of assorted transcription factors (Sp1, Sp3, USp3, NRF-1, and KLF15; added singly or in combination) on hPCFT core promoter activity. Statistics were performed within each transactivation group by Sp1, NRF-1, KLF15, or NRF-1 + KLF15, upon addition of various Sp factors. (**B**) Transactivation of WT hPCFT core promoter (−50/+96) and hPCFT core promoter with the GC-Box consensus sequence mutation (−50/+96/GC-Boxm), upon transfecting with Sp1, NRF-1, or KLF15 singly or in combination. For both panels A and B,

results are presented as mean values ± standard errors from 3 to 11 different experiments. For both panels: ****$p < 0.0001$; **$p < 0.01$; *$p < 0.05$.

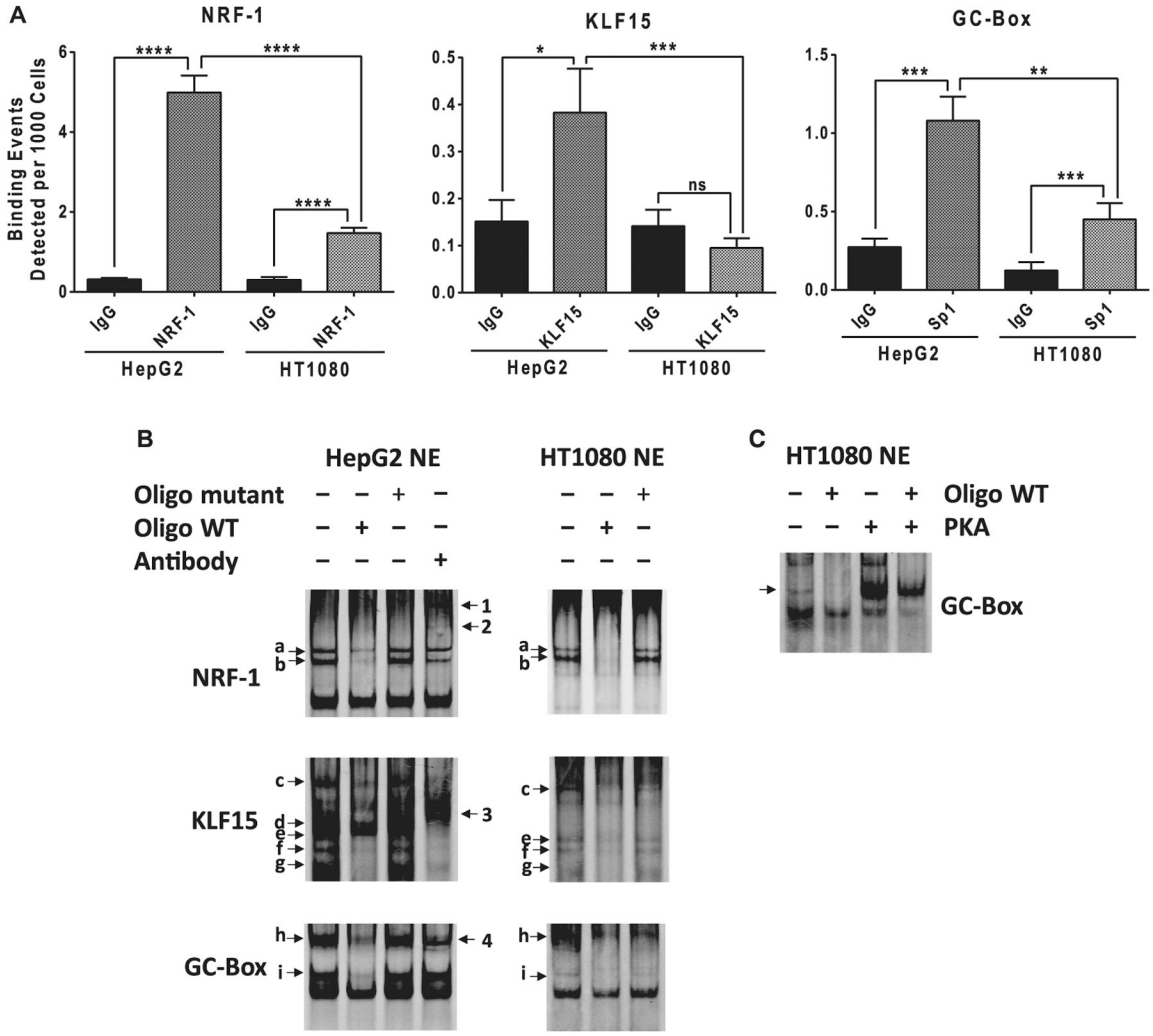

Figure 5. Binding determinations of NRF-1, KLF15 and Sp1 transcription factors to the hPCFT minimal promoter region by ChIP and EMSA assays.

(**A**) ChIP assays were performed in HepG2 and HT1080 cells according to the manufacturer's instructions, with antibodies against NRF-1, KLF15, and Sp1. Mouse IgG2a was used as a negative control in the pull-down step. The ChIP DNA and input DNA were prepared with the ChIP-IT High Sensitivity Kit according to the manufacturer's instructions and were then used for real-time PCR analyses with the 'DNA Standards, Design and Analysis Template' provided with the ChIP-IT qPCR Analysis kit (Active Motif). Real-time PCR was performed using a Roche LightCycler 480 and LightCycler 480 SYBR Green I Master kit, with primers located in the hPCFT core promoter region spanning putative binding sites for NRF-1, KLF15 or Sp1. Statistical analyses were performed using Prism 6.07. Results are presented as mean values ± standard errors from at least three independent experiments of triplicate measurements. ****$p < 0.0001$; **$p < 0.01$; *$p < 0.05$; ns, non-significant. (**B**) NE proteins from HT1080 and HepG2 cells were pre-incubated at room temperature in a reaction solution containing poly(dI-dC) (for binding assay of KLF15 and Sp1) or poly (dA-dT) (for binding assay of NRF-1). WT or mutant competitor oligonucleotides (500 nM for NRF-1 and KLF15 and 50 nM for Sp1) were then added as

appropriate, followed by the addition of IRDye700-labeled duplex oligonucleotide. For supershift experiments, 1~2 μg of antibody to NRF-1, KLF15 or Sp1 was added to the reaction mixtures and incubated for 20 min at 4°C (for NRF-1 and KLF15) or 40 min at 25°C (for Sp1). DNA–protein complexes supplemented with Orange Loading Dye were then separated on 5% TGE native acrylamide gel at 4°C and 80 V. DNA–protein complexes were visualized by an Odyssey infrared imaging system. (**C**) HT1080 NE proteins were incubated with or without protein kinase A catalytic subunit and 10 μM ATP at 30°C for 1 h. Five micrograms of the treated NE proteins were used for EMSA in the presence or absence of WT competitor oligonucleotide.

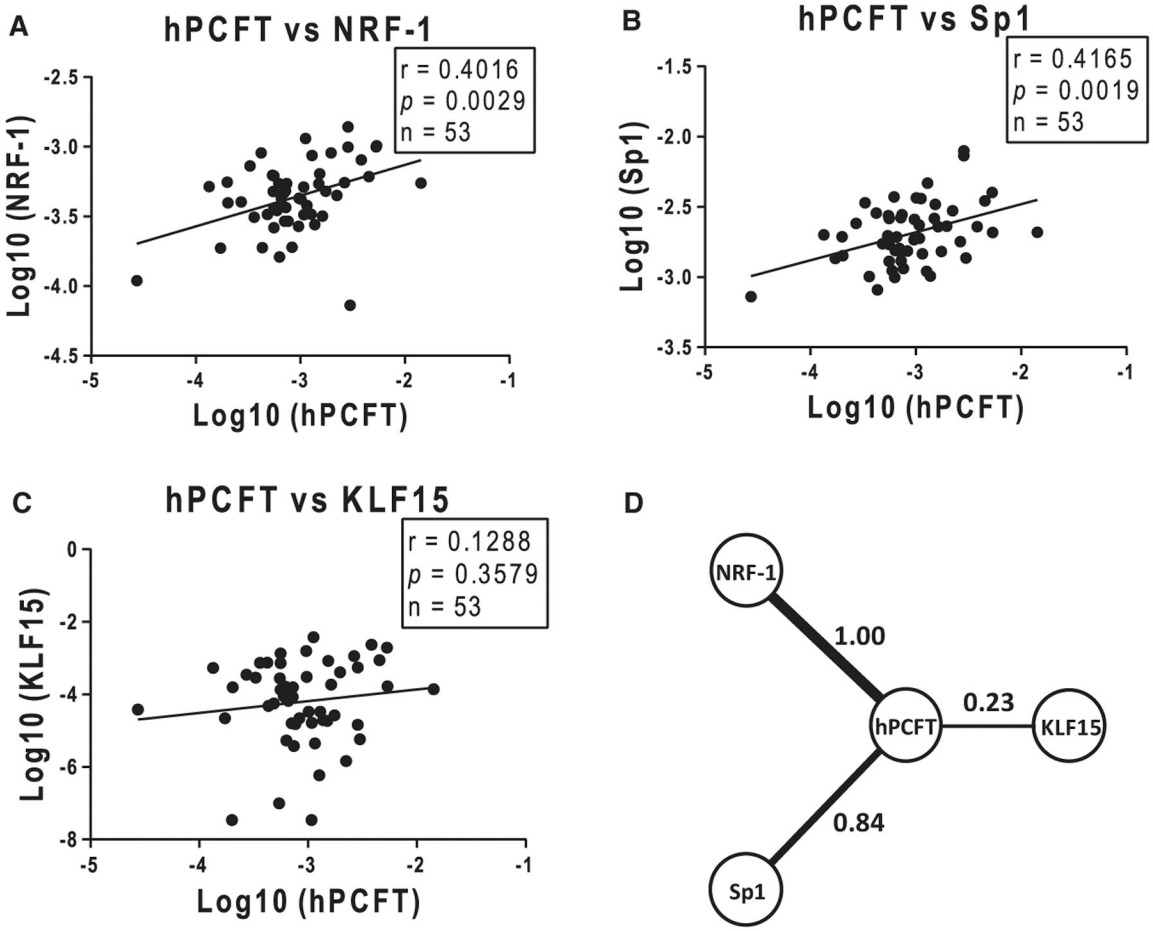

Figure 6. Expression and regulatory associations between hPCFT and NRF-1, Sp1, or KLF15 in solid tumor cell lines.

Transcript levels for hPCFT, NRF-1, Sp1, and KLF15 were measured with 53 solid tumor cell lines studied previously [3] (Supplementary Table S4) by real-time RT-PCR with LightCycler 480 SYBR Green I Master kit. The hPCFT, NRF-1, Sp1, and KLF15 transcript levels were normalized to transcript levels for GAPDH. The scatter plots show univariate associations between hPCFT and NRF-1 (**A**), hPCFT and Sp1 (**B**), and hPCFT and KLF15 (**C**) by Pearson's correlation coefficients (*r*). The x-axis and y-axis scales are logarithmic and the solid gray lines represent the fitted regression lines. N indicates the sample size (53). (**D**) depicts the multivariate regulatory association network between hPCFT and the major transcription factors (NRF-1, Sp1, or KLF15) described in this report, which was inferred by the MRNETB method with Pearson's correlations [28,29]. For the schematic shown, the thickness of the edge and the corresponding numbers (which range from 0 to 1) represent the relative strength of the association. The R/Bioconductor packages *minet* and *igraph* were used to generate the inferred regulatory network [28,29].